Taylor & Francis
Taylor & Francis Group

REVIEW PAPER

The bonded-particle model as a tool for rock mechanics research and application: current trends and future directions

David Oskar Potyondy*

Itasca Consulting Group, Inc., Minneapolis, MN, USA

We generalize our view of a bonded-particle model (BPM) to consist of a base material (that is a packed assembly of rigid grains joined by deformable and breakable cement at grain–grain contacts) to which larger-scale joints can be added and whose mechanical behavior is simulated by the distinct-element method using the two- and three-dimensional discontinuum programs PFC2D and PFC3D. The micromechanical processes that control brittle fracture, and thus, should inform any micromechanical theory or model, are summarized. The rich variety of microstructural models that can be produced by the bonded-particle modeling methodology are described and classified with respect to their microstructural and larger-scale features. These models provide a wide range of rock behaviors that encompass both compact and porous rock at both an intact and rock-mass scale, and examples are provided of how BPMs are being used to model rock at these scales. The examples include an intact anisotropic material that may swell and contract in response to changes in saturation, the behavior of two alternative BPMs that can match both the uniaxial and tensile strengths of compact rock and the embedding of an intact BPM within a larger continuum model to study fracturing around a gold-mine stope in quartzite.

Keywords: bonded-particle model; rock fracture; micromechanics

1. Introduction

As rock-mechanics practitioners, we all have an interest in understanding the mechanical behavior of rock, and we are all aware that rock is much more complex than most traditional engineering materials. In his preface to the fourth edition of *Fundamentals of Rock Mechanics* (Jaeger, Cook, & Zimmerman, 2007), Robert Zimmerman lists topics that are either unique to rock or that assume great importance for rock:

> friction along rough surfaces, degradation and failure under compressive loads, coupling between mechanical deformation and fluid flow, the effect of cracks and pores on mechanical deformation, and, perhaps most importantly, the effect of fractures and joints on large-scale rock behavior.

Modeling provides a means of understanding such complexity via simplification as suggested by the following analogy between two men. In William Stafford's poem (Stafford, 1998) "What's in My Journal," the author strives to understand his inner world via journaling:

> Clues that lead nowhere,
>   that never connected anyway.
> Deliberate obfuscation,
>   the kind that takes genius.

In this paper, the author strives to understand the complexity of rock via modeling:

> Clues that spawn understanding,
>   arrived at by modeling.
> Deliberate simplification,
>   the kind that gives clarity.

The need for simplification in rock-mechanics modeling is stressed by Starfield and Cundall (1988), who suggest that

> . . . we build models because the real world is too complex for our understanding; it does not help if we build models that are also too complex. The art of modelling lies in determining what aspects of the geology are essential for the model.

What is an appropriate model of rock, and how can such a model be developed? Perhaps an *ab initio* model of rock could be constructed.

> A calculation is said to be *ab initio* (or "from first principles") if it relies on basic and established laws of nature without additional assumptions or special models. For example, an *ab initio* calculation of the properties of liquid water might start with the properties of the constituent hydrogen and oxygen atoms and the laws of electrodynamics. From these basics, the properties of the isolated individual water molecules would be derived, followed by computations of the interactions of larger and larger groups of water molecules, until the bulk properties of water had been determined. (Wikipedia, 2012)

In principle, one could construct an *ab initio* model of rock by representing the processes occurring at the atomic

*Email: dpotyondy@itascacg.com

scale using a molecular dynamics (MD) approach (Rapaport, 2004) – the distinct element method can be classified as being analogous to MD modeling, although the constituent particles are no longer the atoms and molecules of MD (Potyondy, 2010a); however, current computing power limits the size of the atomic ensemble to numbers of atoms and molecules that are too small to be useful for most engineering-scale systems (Krajcinovic, 2000) and, in particular, for rock masses on the scale that appears in engineering and mining work. Such accessible rock masses are broken up by structural features, notably joints, that have an important influence on the mechanical behavior, and lead us to consider the rock mass as being composed of intact rock and joints. By adopting representations at larger scales, *particle models* that mimic the microstructural features of intact rock as well as the larger-scale joints can be created and executed in reasonable times on standard desktop computers. Such models are based on the premise that the mechanical behavior of a rock mass is controlled by the orientations and properties of the joints as well as the microstructure of the intact rock material, and complex macroscopic behaviors, such as rupture and sliding along joints as well as fracture and flow of intact rock, arise from structural and microstructural interactions; thus, if one could replicate the joints, the microstructure, and the microstructural interactions within a model, then that model should reproduce the macroscopic behaviors. For the purposes of studying the dominant fracture and failure behaviors of intact rock in the brittle regime, a representation at the grain scale should be sufficient, because the damage processes either occur at this scale or their effects can be mapped to this scale. The bonded-particle model for rock is such a particle model, and the developments reviewed here are guided by the premise that a closer match to the structural and microstructural features will provide a closer match to the real macroscopic behavior.

Such a matching process must be sensitive to scale – i.e., after selecting the scale of the model, then one must select the structural and microstructural features relevant at that scale. The interaction of such features captures the integrated effect of processes occurring at lower scales. This is the approach adopted here. The challenge is to keep the models as simple as possible by including only the features necessary to allow the important mechanisms to occur. Such mechanisms might include rupture and sliding along joints, rupture and sliding along grain–grain interfaces, fracture of grains, and collapse of initial porosity. The idea is sketched in Figure 1. Suppose that we wish to create an excavation in a blocky rock mass. Let us be quite clear about why we are building this model and what questions we are trying to answer. If we are investigating how the intact rock blocks could collapse, then the important mechanism may be rupture and sliding
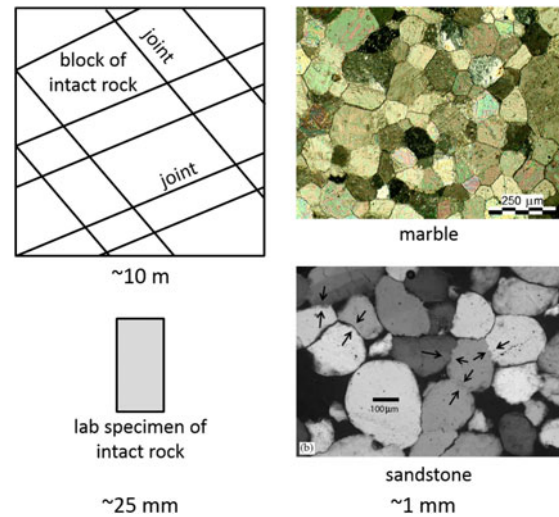

Figure 1. Structural and microstructural features considered in bonded-particle modeling at the rock-mass and lab-specimen scales. The marble image is from Figure 3(a) of Bandini, Berry, Bemporad, and Sebastiani (2012), and the sandstone image is from Figure 23(b) of Haimson (2007). The marble is from an outcrop in Tuscany and was formed by contact metamorphism from a limestone that resulted in a complete static recrystallization of the limestone to give a granoblastic texture of regularly shaped grains with straight boundaries and triple points. The sandstone is a lower-porosity (11–12%) Saint Peter sandstone with broad grain sutures indicated by arrows.

along the joints and the intact blocks can be treated as rigid. If we wish to expand the scope of our investigation to include how the intact rock blocks could fragment, then an additional important mechanism is fracture of the intact blocks, and the fracturing mechanisms must be considered when selecting the appropriate microstructural features. Each intact block can be treated as an assembly of deformable and breakable grains that interact along deformable and breakable grain–grain interfaces. For a compact rock such as the marble, the grains might be perfectly interlocked polygons with no initial porosity, whereas for a porous rock such as the sandstone, the grains might be loosely packed subrounded shapes with substantial initial porosity. Both models for the intact rock would allow fracture of the intact blocks consisting of rupture and sliding along grain–grain interfaces and fracture of grains, but the sandstone model would also allow for the collapse of initial porosity.

The above example also demonstrates that macroscopic behavior of intact rock can be sensitive to subtle microstructural differences. Haimson (2007) reviews drilling experiments in granites, limestones, and sandstones that revealed similar breakout characteristics and strikingly different micromechanisms. Boreholes were drilled into prismatic rock blocks subjected to true triaxial stress intended to replicate field conditions, and breakouts were produced by the removal of loose grains and grain

fragments by the circulating drilling fluid. The quartz-rich sandstones, such as the Saint Peter sandstone shown in Figure 1, have subrounded grains bonded primarily by contact suturing. These sandstones develop tabular slot-shaped breakouts aligned perpendicular to the maximum compressive stress direction. Just ahead of the breakout tip, grain contact loosening and repacking is observed, while grain damage can vary from none in the higher-porosity (18–22%) sandstones to thorough cracking and crushing in the lower-porosity (11–12%) sandstones. Why does the grain damage vary in this way? Haimson (2007) provides the following explanation for the difference in grain damage:

> Grains in the higher-porosity sandstone are sutured along narrow areas of contact (they could be described as practically spot sutures); grains in the lower-porosity rock are sutured almost all around. Thus, in the high-porosity variety grains will debond as soon as the far-field stresses are sufficient to crack the narrow sutures. In the lower-porosity rock the thorough quartz overgrowth inter-granular sutures render the grain bonds practically equal in strength to that of the quartz grains. Hence, the far-field stresses necessary to fail the sutures also induce grain crushing.

Thus far, we have envisioned a rock mass in terms of structural and microstructural features relevant at a specific scale. An alternative means of envisioning a material is suggested by van Mier (2007) in the form of fracture potentials (force-separation relations) at various observation scales, from atomistic and molecular to macroscopic. The virtual material consists of spherical particles with the fracture potential describing the interactions at the contact points between the particles. The fracture potential at a particular scale is caused by the physical mechanisms occurring at that scale (e.g., capillary water forces at the scale of cement, sand or clay particles). The virtual material consists of particles in contact, and the interaction laws form the constitutive equation. In this material, the structural and microstructural features are not modeled directly; instead, their emergent mechanical behavior is captured in the fracture potential. Similar reasoning underlies the application of bonded-particle models to simulate boundary-value problems in which the grains are made much larger than the actual grains (see Section 4.3).

A similar alternative means of envisioning a material is provided by the lattice scheme of Cundall (2011), which is a simplification of the bonded-particle model in which the finite-sized particles are replaced by point masses, and the contacts between particles are replaced by springs that may break. Cundall's lattice scheme is well suited to model fracturing of a brittle solid in 3D that contains existing discontinuities, and for which failure initiation occurs at small strains, typically much less than 1%. For such systems, the lattice scheme achieves high computational efficiency because the interaction geometry, consisting of the location and apparent stiffness of springs, can be pre-computed, eliminating contact detection as an overhead. The simplifications, however, come at the price of restricting model applicability to rock-mass response in which the intact rock failure is by tensile fracture; reproducing the strength envelope of intact rock requires a more complex contact law and microstructure, as provided by the bonded-particle model.

The remainder of the paper is organized as follows. The microstructural physics of intact rock is discussed in Section 2 by summarizing the micromechanical processes that control brittle fracture, and thus, should inform any micromechanical theory or model. It is suggested that the BPM provides a micromechanical theory of brittle failure in the form of a computational model; although not amenable to theoretical treatment in the same way as a traditional theory, the BPM provides various physical models of the brittle fracture process that are amenable to computation, and from which one can discern the effects of the microstructure on the macroscopic behavior. The question of how one can sanction (or gain confidence in) such a micromechanical model is also addressed.

The bonded-particle modeling methodology is described in Section 3. The development and application of the methodology are described in the first subsection. Then a definition and generalization of the methodology are provided in the next three subsections, which begin by defining the PFC model, which includes both granular and bonded materials, and noting that the BPM is a bonded material. We then generalize our view of the BPM to consist of a base material to which larger-scale joints can be added. Finally, the rich variety of microstructural models that can be produced are described and classified with respect to their microstructural and larger-scale features.

Examples of how BPMs are being used to model rock at both an intact and rock-mass scale are provided in Section 4. Such models attempt to replicate the relevant microstructural and larger-scale features; however, the determination of what is relevant depends upon the intended use of the model. Such uses might include scientific investigations of: the damage processes in argillaceous materials that may swell or contract in response to changes in saturation (see Section 4.1), the spalling phenomenon in hard rock (see Section 4.2), or the fracturing processes surrounding a gold-mine stope in quartzite (see Section 4.3). In the second case, a direct representation of the grains and interfaces at their true sizes may be necessary, whereas in the first and third cases, an indirect representation of notional grains and interfaces of a size much larger than the true grain size may be sufficient.

The current limitations of bonded-particle modeling along with suggested avenues for further development are discussed in Section 5 where it is suggested that future

BPMs should be constructed to match particular rock types such as granite, limestone, or sandstone.

2. Microstructural physics of intact rock

BPMs are used to model rock at both an intact and rock-mass scale by viewing the intact rock as a base material upon which larger-scale joints may be added. When considering the behavior of the rock mass, the orientation and sliding of the joints may be relevant as suggested by Jaeger et al. (2007):

> The loads applied to a rock mass are generally due to gravity, and compressive stresses are encountered more often than not. Under these circumstances, the most important factor in connection with the properties and continuity of a rock mass is the friction between surfaces of cracks and joints of all sizes in the rock. If conditions are such that sliding is not possible on any surfaces, the system may be treated to a good approximation as a continuum of rock, with the properties of the average test specimen. If sliding is possible on any surface, the system must be treated as a system of discrete elements separated by these surfaces, with frictional boundary conditions over them.

When considering the possibility of fracture of the intact rock between the joints, the microstructural physics is relevant. In this section, we summarize those aspects of the microstructural physics of intact rock that should inform the construction of a BPM. An attempt is made to simplify this topic so as to provide a conceptual framework for the use of BPMs (which requires the selection of an appropriate model), the sanctioning of a particular BPM (which requires a calibration process in which a particular instance of a BPM is used to simulate a set of material tests so as to reproduce the relevant macroscopic properties – these material tests may include field-scale response such as excavation-induced damage), and the ongoing development of BPMs. Paterson and Wong (2005) and Jaeger et al. (2007) provide comprehensive discussions of the mechanical behavior of intact rock, and Jaeger et al. (2007) discuss rock-mass behavior as well. Much of the material in this section borrows heavily from these two texts.

Intact rock can be classified into the three categories: igneous, sedimentary, and metamorphic. Igneous rocks consist of a crystalline assemblage of minerals that have crystallized from molten rock or magma (examples include granite and basalt). Sedimentary rocks consist of an assemblage of detrital particles bound together in a matrix of finer materials (examples include sandstone, limestone, and shale). Metamorphic rocks consist of igneous or sedimentary rocks that have undergone chemical, mineralogical, or textural changes due to extremes of pressure and/or temperature (examples include gneiss, marble, and quartzite).

The mechanical structure of rock presents several different appearances, depending upon the scale (intact or rock-mass) at which it is studied. We focus on intact rock in the present discussion. Intact rock can be viewed as an aggregate of crystals and amorphous (i.e., occurring in a mass, as without stratification or crystalline structure) particles joined by varying amounts of cementing materials. The crystals generally have dimensions of the order of centimeters or less and represent the smallest scale at which the mechanical properties are studied. The mechanical properties of intact rock are measured by performing laboratory tests on rock specimens having dimensions of centimeters and containing a sufficient number of crystals and structural particles for them to be regarded as grossly homogeneous. Although the crystals and particles may differ widely from one another, they interact in a sufficiently random manner so as to imbue the specimen with average homogeneous properties, which may be anisotropic because of the rock fabric – e.g., bedding planes in a sandstone.

Paterson and Wong (2005) summarize the state of current knowledge of the brittle mechanical properties of rock as determined in laboratory experiments on relatively small specimens of intact rock. The distinction between brittle and ductile behavior is a macroscopic one, depending on whether or not the rock specimen is capable of undergoing substantial permanent strain without macroscopic fracture, which is described as "brittle fracture" when it is not preceded by any appreciable amount of permanent deformation. The brittle mechanical properties are those of the rock material; different, and perhaps even ductile, mechanical properties are those of the rock mass, which often contains joints at a scale larger than that of the specimen. Many types of tests have been used in the experimental study of brittle fracture in rock. Paterson and Wong consider mainly the results from the uniaxial compression test and the conventional triaxial test, because the applied homogeneous stress makes their interpretation relatively simple, and allows them to define the brittle fracture stress as the peak axial stress during such tests.

Paterson and Wong distinguish two principal modes of brittle failure: *shear fracture*, in which the relative displacement is parallel to the fracture surface, and *extension fracture*, in which the relative displacement is normal to the fracture surface. The shear fracture is the dominant mode of macroscopic brittle failure in triaxial compression tests (at all but the lowest confining pressures), in which the shear fracture is aligned $20-30°$ to the compression axis. As the brittle–ductile transition is approached with increasing confining pressure, the shear fracture tends to become a zone of intense deformation and fine-scale fracturing, rather than a well-defined planar feature, and specimen separation may not then take place readily at the failure zone after the test. The extension fracture is the dominant mode of macroscopic brittle failure in direct-tension tests, in which the extension

fracture is aligned normal to the tension axis. Extension fractures also occur under macroscopically compressive conditions (e.g., triaxial extension, Brazilian and compression tests with very low confinement) in the form of splitting parallel to the compression axis. An explanation of why this axial splitting occurs is provided in Section 2.2.

The brittle mechanical properties of intact rock are controlled by the nature of its pore space; therefore, we classify intact rock as either *compact* or *porous*. Compact rock has very small porosity, less than a few percent, while porous rock has a substantial amount of pore space, especially as intergranular space. Compact rock has a crack-like pore space, while porous rock has a more open pore space. Compact rock includes igneous, low-porosity sedimentary, and high-grade metamorphic types, while porous rock includes high-porosity sedimentary and low-grade metamorphic types. We use the term "microcrack" to include all cracks on the microscopic scale, from dimensions of several grain diameters down to a fraction of a grain diameter – see Kranz (1983) for an extensive review of microcrack morphology and classification. Microcracks tend to be ubiquitous in all rocks, and they may be the main source of porosity in compact rock. Examples of microcracks include cleavages and other fractures in mineral grains and partings at originally intact grain boundaries. There are a rich variety and abundance of microcavities (pores and microcracks) in virgin compact rocks, especially in granites, where long, narrow, and sharp-ended cracks are rarely seen; instead, blunt-ended elongate cavities occupy a large proportion of the grain boundaries (Paterson & Wong, 2005, Section 5.7.3).

The damage processes of intact rock differ under compressive or tensile loading conditions (Meredith, 1990). *Under slowly increasing compressive loading*, numerous microcracks nucleate and propagate primarily as tensile (mode I) cracks in a direction parallel to the compression axis. A number of nucleation mechanisms have been suggested, including stress concentrations at pre-existing flaws, elastic mismatch between contacting grains which produces tensile stresses along the surface of the stiffer grain, and sliding along pre-existing microcracks which produces wing cracks at their tips. Application of even a modest confining stress causes individual microcracks to extend in a stable manner, extending just enough to relieve the local stress concentration and then arresting. As the differential compressive stress is increased, an increasing population of microcracks extends until they interact with each other to produce a shear fracture. *Under slowly increasing tensile loading*, very few microcracks nucleate or propagate. Either an existing microcrack propagates unstably or a microcrack nucleates from a flaw and then propagates unstably to produce an extension fracture.

Compressive failure is a cooperative process involving the nucleation, stable growth, and eventual interaction of many microcracks to produce a shear fracture, whereas tensile failure is an independent process involving the unstable growth of a single microcrack. This last statement is overly simplistic: in many rocks and in concrete, in particular, a process zone forms and provides stress bridging across the surfaces of the growing extension fracture. A more accurate statement would be that tensile failure is far less stable than compressive failure.

Compression-induced damage of intact rock manifests itself as inelastic volume change (dilation or compaction) resulting from microstructural changes that are precursors to macroscopic failure. Such changes involve cracks and pores and are an important aspect of the deformational behavior of granular aggregates and rock. Granular aggregates exhibit dilatancy when subjected to deviatoric loading, and this dilatancy is attributed to repacking of the grains. Compact rocks exhibit dilatancy when subjected to deviatoric loading, and this dilatancy is attributed to microcracking occurring prior to macroscopic failure. The behavior of porous rocks is more complex, because the pore space plays a significant role in the destruction of cohesion between grains and in compaction. Inelastic volume changes in porous rocks occur during both hydrostatic and deviatoric loading. When subjected to hydrostatic loading, porous rocks may exhibit compactancy which is attributed to grain crushing. When subjected to deviatoric loading, the collapse of porosity tends to counterbalance the tendency to dilatancy noted above for compact rock, and so porous rock may exhibit compactancy (often called "shear-enhanced compaction") which is attributed to either brittle grain crushing or ductile plastic collapse of the pores.

The microstructural processes that occur in intact rock subjected to compressive loading are described by the synoptic view of brittle failure (Paterson & Wong, 2005, Section 5.8), in which the stress–strain behavior of a compact rock in compression in the brittle field is divided into several stages prior to macroscopic failure (see the left side of Figure 2): (I) a "settling down" phase, (II) nearly perfect linear elasticity, (III) development of microfracturing and dilatancy involving stable microcrack propagation, and (IV) unstable developments in the pattern of microcracking, involving localization and leading to the growth of a macroscopic fracture. A similar descriptive framework derives from the work of Martin and Chandler (1994) and is summarized on the right side of Figure 2 in terms of characteristic stress levels (crack initiation, crack damage, and peak strength) occurring during a compression test; these characteristic stress levels are important in understanding the damage process and in calibrating and sanctioning a BPM.
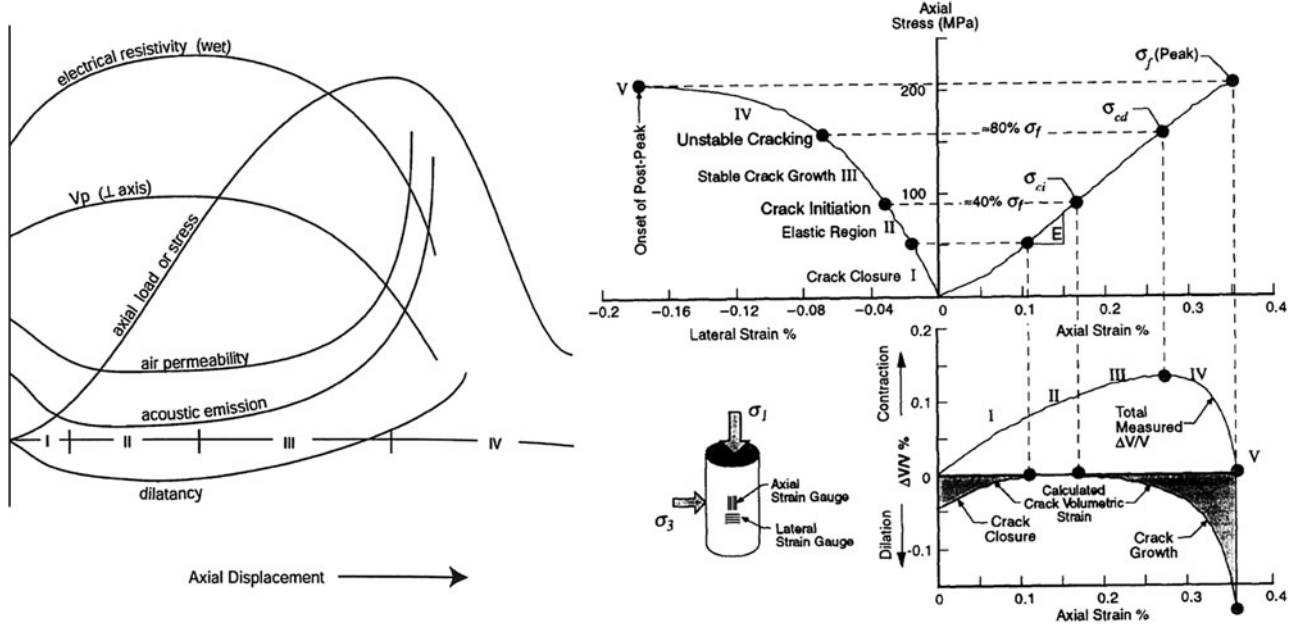
Figure 2.   Generalized demarcation of four stages in the complete load-displacement curve of a compact rock in a compression test and the corresponding changes in various physical properties [left, from Figure 45 of Paterson and Wong (2005)]. Stress–strain curves of a typical compact rock (Lac du Bonnet granite) showing the stages of damage development [right, from Figure 1 of Martin and Chandler (1994)].

2.1.   Brittle failure behavior of rock

In the next two bullets, we summarize the brittle failure behavior of compact rock using granite as an example. The summary borrows freely from Paterson and Wong (2005, Section 5.7.4) and is intended to be used for the calibration and sanctioning of BPMs of intact compact rock. Work is only now beginning to develop BPMs of intact porous rock; thus, the third bullet summarizes the brittle failure behavior of porous rock.

- In uniaxial compression of granite, substantial microcracking is evident before the peak stress is reached. The microcracks are both intergranular and transgranular, and are distributed throughout the specimen. Most of the microcracks are parallel to the specimen axis but some are inclined up to 35° to the axis, and the proportion of more highly inclined microcracks increases as the total microcrack density increases with progression toward and through the peak stress. The following microstructural changes occur at the point where dilatancy is first detected: (1) an increase in the amount of grain boundary cracking, both through rupturing of bridges in the original elongate cavities and through the appearance of new elongate cavities, so that most grain boundaries are almost continuously cracked before the peak stress is reached; (2) completely healed microcracks are reopened; and (3) a few fresh cleavages appear in the microcline.

At somewhat higher stress, transgranular axial microcracks begin to proliferate, starting at pores, at transverse grain boundaries between different minerals and at pre-existing elongate cavities at grain boundaries. At the higher stress, the transgranular microcracks tend to run from grain boundary to grain boundary so that at the peak stress, nearly all grains contain new transgranular cracks. Only after passing the peak stress does local shear fracturing become obvious microscopically, with shear fractures developing on a macroscopic scale before macroscopic axial splitting occurs as the final stage of specimen collapse.

- In confined-compression of granite, application of confining pressure in the range up to 150 MPa leads to more profuse pre-failure microcracking and, except at very low confining pressures, this increase results from an increase in the proportion of microcracks inclined at 20° or more to the specimen axis. Below 10 MPa confining pressure, the peak stress is still associated with the proliferation and growth of predominantly axial microcracks, but the macroscopic axial splitting that tends to develop in uniaxial tests is suppressed. At higher confining pressures, (a) the microcracks (now mainly inclined ones) tend to form inclined zones which develop into the macroscopic shear fracture, often by linking up en echelon inclined fractures and (b) the localized coalescence of microcracks that extend

over two or more grains is quite evident in samples loaded beyond the peak stress.

- The brittle failure behavior of porous rock involves micromechanical processes quite different from, and more complex than, those in compact rock. Most studies have focused on sandstone. In a porous sandstone, the development of brittle failure is different in at least three aspects (Paterson & Wong, 2005, p. 114): (1) While the phenomenological behavior is qualitatively similar to that shown in Figure 2, the permeability evolution may be significantly different – the permeability may actually decrease while a porous sandstone undergoes dilatancy with the transition in permeability evolution occurring at a porosity of about 15%. (2) Stress-induced microcracking is not as pervasive in porous rock. In Stage III, the acoustic emission activity seems to be associated with the rupture of lithified grain contacts, and dilatancy arises primarily from the relative movement among grains. Microcracks that proliferate in Stage IV are mostly extensile microcracks emanating from grain contacts and assumed to be caused by Hertzian contact stresses. (3) While shear localization involves the coalescence of clusters of such Hertzian cracks, its development in Stage IV depends on the interplay between dilatant and compactive processes.

2.2. The BPM as a micromechanical theory of brittle failure

Before arguing that the BPM provides a micromechanical theory of brittle failure, we consider the question of why

axial splitting occurs. This allows us to introduce the essential features of a BPM and compare the BPM with an alternative idealization of the rock.

As stated above, extension fractures occur in uniaxial compression tests in the form of splitting parallel to the compression axis. *Why does axial splitting occur?* We offer an explanation that follows from either of two complimentary idealizations of the rock, which we will denote as LEFM and BPM materials. The accepted explanation is that *axial splitting originates from local transverse tensile stresses at flaws or heterogeneities in the rock.* Such stresses arise in a continuous material (idealized as a linear-elastic body with an initial population of micro-cracks for which the behavior follows from linear elastic fracture mechanics, LEFM) at the tips of inclined microcracks. Such stresses also arise in a cemented granular material (idealized as a bonded-particle model, BPM and shown in Figure 3) in which the macroscopically applied compressive load is carried by the grain and cement skeleton in the form of force chains that propagate from one grain to the next across grain–grain contacts and thereby induce many sites of microtension oriented perpendicular to the direction of compressive loading (for the reasons shown in Figure 4). For both materials, the extension fractures nucleate (as wing cracks in the LEFM material and as broken bonds in the BPM material) and then grow (as lengthening cracks in the LEFM material and as additional broken bonds that coalesce into extension fractures in the BPM material) into an orientation parallel to the direction of compressive loading.

Notice that by idealizing the rock in terms of grains and cement directly, the BPM material provides a mechanism for microcrack nucleation as well as growth and eventual
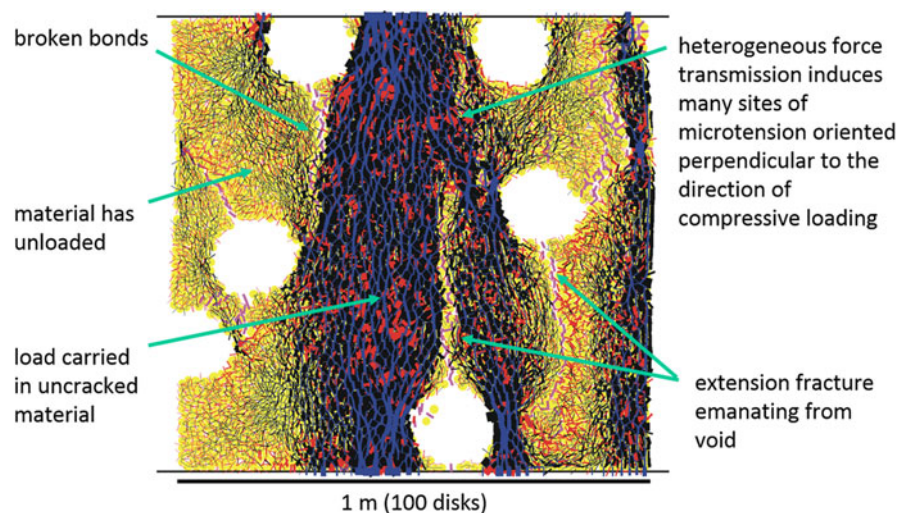

Figure 3. (Colour online) Force-chain fabric and broken bonds (magenta) in a cemented granular material idealized as a parallel-bonded BPM in the post-peak portion of a uniaxial compression test. Blue is grain–grain compression, while black and red are compression and tension, respectively, in the cement drawn as two lines at the bond periphery. Line thicknesses and orientations correspond with force magnitude and direction, respectively, and the moment in the cement contributes to the forces at the bond periphery.
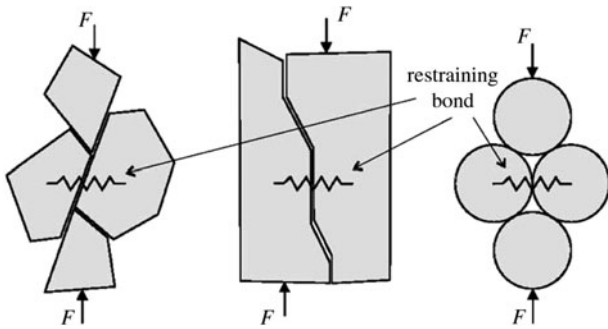
Figure 4. Microstructural mechanisms in a cemented granular material that induce microtension oriented perpendicular to the direction of compressive loading. Breakage of the restraining bond creates a microcrack oriented parallel to the direction of compressive loading.

interaction. The grain-scale discontinuities in the BPM material provide the "flaws and heterogeneities" mentioned earlier, and such discontinuities differ from the microcracks in the LEFM material. The BPM material may be more appropriate for modeling the physical behavior mechanisms of rock than the more simplified LEFM material, because the BPM material supports a richer set of grain-scale discontinuities that can be related to microstructural features. For the LEFM material, all microstructural features must be mapped into an initial population of microcracks.

The behavior of intact rock subjected to compressive loading is *described* by Paterson and Wong (2005) in Figure 2. The behavior is *explained* by Paterson and Wong in terms of flaws and heterogeneities in the rock material on the microscopic scale in which brittle fracture is viewed as a localization in the proliferation of microcracking. Paterson and Wong (2005, p. 57) stress that "... it is essential to have a realistic structural description of the rock as a basis for ... theoretical developments, and to consider the evolution of the structure during the progression of the failure." They suggest that such theoretical developments take the form of a *micromechanical theory of brittle failure* which postulates a physical model of the brittle fracture process that is amenable to theoretical treatment. This model attempts to capture the important attributes inferred from microstructural and acoustic emission observations, and to arrive at constitutive relations (which can be viewed as criteria of failure applicable to general states of stress) that describe the inelastic and failure behavior observed in experiments. Paterson and Wong (2005, Section 6.1) argue that:

> ... an adequate theory of failure should ... provide a fairly complete description of the key mechanical processes from the stage of initiation [microcrack nucleation] to the final stage of macroscopic fracture ... [and should] take the following aspects into account: (1) The local initiation [or nucleation] of potentially-growing microcracks at source defects. (2) The subsequent individual growth of these microcracks with increased loading. (3) The increase in the

number of growing microcracks with increased loading. (4) The interaction between the growing microcracks as their lengths and numbers increase. (5) The stability of the crack proliferation process and the possibility of its localization, leading to macroscopic failure.

> In compact rock, it is commonly considered that the sources of microcrack initiation [or nucleation] are themselves microcracks already present in the rock and that from the onset of dilatancy ... to near the peak stress, irreversible deformation involves the growth of stress-induced extensile microcracks. A theoretical model should characterize the nucleation and stable propagation [or growth] of the multiplicity of stress-induced microcracks in relation to the evolution of dilatancy and strain hardening behavior. In porous rock, considerations of crack initiation at pores or of intergranular bonding strength also enter ....

> Under overall compressive loading, final macroscopic failure occurs by shear localization. From a micromechanical view, this final stage is dominated by crack coalescence. The mechanics of the coalescence process hinges on the complex interaction of stress fields of the numerous neighbouring cracks. A comprehensive analysis of the evolution of the instability requires fairly detailed characterization of the microcrack structure in conjunction with intensive computation.

The BPM provides such a micromechanical theory of brittle failure. It allows for all of the stated mechanisms, and it can be used in all of these capacities. However, unlike a theoretical model that serves to characterize the damage processes, the BPM does not characterize these processes, and thus is not amenable to theoretical treatment as noted above. Instead, it mimics these processes and their interactions, and thus can be used to discern the effects of the microstructure on the macroscopic behavior. In addition, the BPM can be applied to boundary-value problems at the scale that appears in engineering and mining work to study damage processes around such things as subsurface excavations, mines, and boreholes (see Section 4.3).

A distinction between theoretical and computational models is sometimes made by claiming that theoretical models (in the form of analytical solutions) have the virtue of displaying the effect of parameters of a problem in a clear and transparent way, whereas computational models are best suited to analyze specific boundary-value problems involving complex geometries and constitutive behaviors. This distinction becomes blurred for BPMs, because well-parameterized BPMs can be employed in parameter studies to discern the effect of parameters on the behavior of a modeled system.

2.3. Sanctioning the BPM

No model is complete or fully verifiable (Oreskes, Shrader-Frechette, & Belitz, 1994); instead, the best that can be done is to sanction the model. According to Winsberg (2010, p. 23):

The sanctioning of simulations does not cleanly divide into verification and validation. In fact, simulation results are sanctioned all at once: simulationists try to maximize fidelity to theory, to mathematical rigor, to physical intuition, and to known empirical results. But it is the *simultaneous confluence* of these efforts, rather than the establishment of each one separately, that ultimately gives us confidence in the results.

BPMs of intact rock have been sanctioned by demonstrating that they match the response obtained during direct-tension and compression tests of a typical compact rock. This response consists of the properties measured during such tests (e.g., direct-tension strength, elastic constants, crack-initiation stress, crack-damage stress, and peak strength) as well as the microstructural behavior that occurs during such tests. The microstructural behavior is viewed through the lens of the interpretive framework illustrated in Figure 2, which allows one to relate the model behavior to that of the rock. In some cases, the BPM parameters are chosen to approximate the true microstructural properties, and then the macroscopic behavior is studied. But in most cases, either the true microstructural properties are not known or the BPM is a simplification of the true microstructural features. In such cases, the BPM parameters must be chosen by performing a calibration process in which a particular instance of a BPM is used to simulate a set of material tests, and the BPM parameters are chosen to reproduce the relevant response occurring in such tests. In addition to the laboratory-scale tests noted above, field-scale tests that may include excavation-induced damage have also been used in the sanctioning process.

The behavior of any intact rock can be mapped into the interpretive framework illustrated in Figure 2, but such a mapping is overly simplistic for porous rock. Further research into the microstructural behavior of porous rock that could contribute to an expansion of the interpretive framework is welcome. Nonetheless, this interpretive framework serves as the starting point for calibrating any microstructural model of rock; furthermore, we assert that any microstructural model that matches this response set can be used to study, and make quantitative assessment of, rock damage. This is the philosophy that underlies the ongoing application and development of BPMs. It should be noted that the sanctioning of BPMs of a rock mass is an even more complex undertaking, because it must incorporate the effect of the joints on the system behavior, and there is no interpretive framework similar to Figure 2 for a rock mass. Further development of BPMs would benefit greatly from the development of such a framework.

3. Bonded-particle modeling methodology

The PFC model (defined below) provides a synthetic material consisting of an assembly of rigid grains that interact at contacts and includes both granular and bonded materials as well as an interface that can be inserted into the bonded materials. This synthetic material encompasses a vast microstructural space, and only a small portion of this space has been explored. For example, the bonded-particle modeling methodology, which is the focus of this paper, provides a rich variety of microstructural models in the form of bonded materials. The most up-to-date incarnation of the PFC model is provided in the form of the linear, contact-bonded, parallel-bonded, and flat-jointed materials (Potyondy, 2014). These materials support practical applications (via boundary-value models made from these materials) and scientific inquiry (via further exploration of the microstructural space described earlier).

3.1. Development and application

The development and application of the bonded-particle modeling methodology are discussed in this section. The discussion focuses on the author's own work, and is not meant to be exhaustive; instead, it is meant to both clarify this modeling approach and to aid in its application and further development by others who are using it as a tool in their own work.

The PFC model is a distinct element modeling approach that encompasses both granular and solid materials, and has also been applied to simulate carbon nanotube systems by Ostanin, Ballarini, Potyondy, and Dumitrica (2013). The historical background and characteristic features of the approach are discussed in Lemos (2011). Cundall and Strack (1979) describe the main features of the distinct element method (DEM) applied to simulate the mechanical behavior of unbonded disks and spheres. Such a system behaves like a cohesionless granular material. Potyondy and Cundall (2004) extend the DEM model to include bonding and demonstrate that such a system behaves like a brittle solid material such as rock. Such models are called bonded-particle models or BPMs.

The bonded-particle model for rock was defined by Potyondy and Cundall (2004) to consist of a dense packing of non-uniform-sized circular or spherical particles that are bonded together at their contact points and whose mechanical behavior is simulated by the distinct-element method using the two- and three-dimensional discontinuum programs PFC2D and PFC3D. In their defining paper, the authors argued that (1) rock behaves like a cemented granular material of complex-shaped grains in which both the grains and the cement are deformable and may break, and that such a conceptual model can, in principle, explain all aspects of the mechanical behavior and (2) BPMs can mimic this system and thus exhibit a rich set of emergent behaviors that correspond very well with those of real rock. The emergent behaviors for the case in which the grains are rigid circular or spherical

particles and the cement is a parallel bond include: elasticity, fracturing, acoustic emission, damage accumulation producing material anisotropy, hysteresis, dilation, post-peak softening, and strength increase with confinement.

Potyondy (2007a) extends the BPM to include time-dependent behavior by adding to the parallel-bond formulation a damage-rate law that mimics the stress-corrosion process. Mas Ivars, Potyondy, Pierce, and Cundall (2008) extend the BPM to include joints at a scale larger than the particles by creating a smooth-joint contact model that allows each joint to be represented as a collection of smooth-joint contacts. The development of the smooth-joint contact model allows us to herein generalize our view of the BPM to consist of a base material to which larger-scale joints can be added (see Section 3.3).

A BPM consisting of contact- or parallel-bonded disks or spheres suffers from the limitation that if one matches the unconfined-compressive strength of a typical compact rock, then the direct-tension strength of the model will be too large. This limitation is addressed by: (a) creating a 2D clumped material (Cho, Martin, & Sego, 2007) and (b) enhancing the 2D and 3D parallel-bond contact models (Potyondy, 2011). This limitation is overcome by creating a 2D grain-based model and a 2D and 3D flat-joint contact model (see Section 4.2) as well as by increasing the connectivity of the bonded materials [by installing bonds between all grains with a gap less than a specified installation gap as defined in Potyondy (2014)].

The original BPM has been used to study a wide range of rock-mechanics phenomena including: the effect of lithophysae (hollow, bubble-like voids) on the mechanical properties (Young's modulus and uniaxial compressive strength) of the lithophysal tuff at Yucca Mountain and to quantify the variability of these properties (Potyondy, 2007b); the effects of porosity and crack density on the mechanical properties of rock (Schöpfer, Abe, Childs, & Walsh, 2009); the effects of stress and induced cracking on the static and dynamic moduli of rock (Potyondy & Hazzard, 2008); unstable fault-slip in granite (Hazzard, Collins, Pettitt, & Young, 2002); thermally fractured granite (Wanne & Young, 2008); acoustic emissions and induced seismicity (Hazzard & Young, 2000, 2004); the behavior of rock joints (Asadi, Rasouli, & Barla, 2012; Park & Song, 2009); the structure and growth of faults (Schöpfer, Childs, & Walsh, 2007a, 2007b); the orientation and dilatancy of shear bands (Schöpfer & Childs, 2013); the brittle–ductile transition (Schöpfer, Childs, & Manzocchi, 2013); and fluid injection into granular media (Zhang, Huang, & Damjanac, 2012). This list is not exhaustive. A search of Google Scholar (on 30 October 2014) revealed 38 articles with the name "bonded-particle model" in their title, and 1250 articles that cited the defining paper. No attempt is made here to review or summarize this work.

BPMs with smooth joints (i.e., with joints represented as a collection of smooth-joint contacts) have been used to create the following synthetic materials: a jointed rock-mass (referred to as a Synthetic Rock Mass, see Section 3.4); a 2D grain-based model that mimics deformable, breakable polygonal grains with deformable, breakable grain–grain interfaces (see Section 3.4); and an anisotropic material that may swell and contract in response to changes in saturation (see Section 4.1). BPMs with smooth joints have been applied to study: confinement-dependent rock strength degradation in hard rock (Bahrani, Valley, Kaiser, & Pierce, 2011) and fracture spacing in layered rocks (Schöpfer, Arslan, Walsh, & Childs, 2011).

The clumped material has been applied to study the development of a shear zone (Cho, Martin, & Sego, 2008), dilation and spalling (Cho, Martin, Sego, & Jeon, 2010), and confined asymmetric compression (Yoon, Zang, & Stephansson, 2012) of compact rock. The enhanced parallel-bond contact model has been applied to study the fracturing that occurs around an advancing stope in quartzite (see Section 4.3). The grain-based model has been applied to study spalling (see Section 4.2) and Brazilian-test behavior in compact rock (Bahrani, Potyondy, & Pierce, 2012). The 2D flat-joint contact model has been applied to study the rock disaggregation process occurring near a wellbore perforation in sandstone (Potyondy & Xiao, 2014).

3.2. PFC model

The PFC programs (PFC2D and PFC3D) provide a general purpose, distinct-element modeling framework that includes a computational engine and a graphical user interface (Itasca Consulting Group, Inc, 2014a). A particular instance of the distinct-element model is referred to as a *PFC model*, which refers to both the 2D and 3D models. The PFC model simulates the movement and interaction of many finite-sized particles. The particles are rigid bodies with finite mass that move independently of one another and can both translate and rotate. Particles interact at pair-wise contacts by means of an internal force and moment. Contact mechanics is embodied in particle-interaction laws that update the internal forces and moments. The time evolution of this system is computed via the distinct-element method, which provides an explicit dynamic solution to Newton's laws of motion.

We here generalize and expand upon the definition of the PFC model given above. The PFC model simulates the movement of particles and their mechanical interaction at pair-wise contacts. We denote each particle as a *body* to clarify that it is not a point mass, but instead is a rigid body with finite mass and a well-defined surface. The PFC model consists of bodies and *contacts* (see Figure 5).
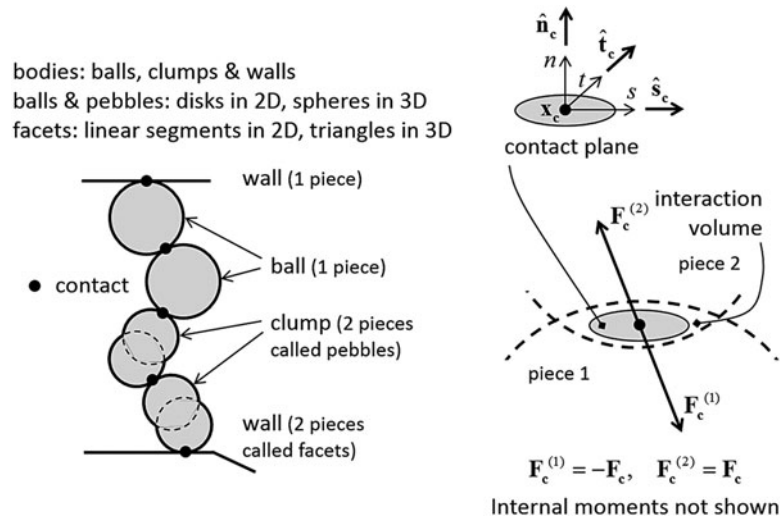
Figure 5. PFC model showing bodies and contacts (left) and contact plane with internal force (right).

There are three types of bodies: *balls*, *clumps*, and *walls*. Bodies have surface properties that are assigned to the *pieces* on the body surface. A ball consists of one piece, which is the ball itself, while the pieces of a clump and wall are called *pebbles* and *facets*, respectively. A ball is a rigid unit-thickness disk in 2D or sphere in 3D. A clump is a collection of pebbles that are rigid unit-thickness disks in 2D or spheres in 3D. Clumps model arbitrarily shaped rigid bodies. The pebbles comprising a clump can overlap but contacts do not exist between them; instead, contacts form between the pebbles on the boundary of a clump and other bodies. A wall is a collection of facets that are linear segments in 2D or triangles in 3D and that form a manifold and orientable surface.

Contact mechanics is embodied in particle-interaction laws that employ a soft-contact approach for which all deformation occurs at the contacts between the rigid bodies. The mechanical interaction between the surfaces of two bodies occurs at one or more pair-wise mechanical contacts. Contacts are created and deleted based on body proximity by the contact-detection logic. A contact provides an interface between two pieces. The interface consists of a contact plane with location ($\mathbf{x_c}$), normal direction ($\hat{\mathbf{n}_c}$), and coordinate system (*nst*). The contact plane is centered within the interaction volume (either gap or overlap) of the two pieces, oriented tangential to the two pieces and rotated to ensure that relative motion of the piece surfaces remains symmetric w.r.t. the contact plane. Each contact stores a force ($\mathbf{F_c}$) and moment ($\mathbf{M_c}$) that act at the contact location in an equal and opposite sense on the two pieces. The internal force and moment are updated by the particle-interaction law, which takes the relative motion and surface properties of the two pieces as input. We refer to the particle-interaction law as a *contact model*.

3.3. Generalization of the BPM

We generalize our view of the BPM to consist of a *base material* to which larger-scale *joints* can be added. The base material consists of a packed assembly of rigid grains joined by deformable and breakable cement at grain–grain contacts with the grains and cement being the bodies and contacts, respectively, of the PFC model (see Figure 6). The grains of the base material can be either balls or clumps drawn from a general grain-size distribution. It is the type of contact model at the grain–grain contacts that defines the material as being contact-bonded, parallel-bonded, or flat-jointed. A smooth-jointed interface (defined at the end of this section) can be inserted into these materials. We here summarily describe only the parallel-bonded and flat-jointed materials – see Potyondy (2014) for a comprehensive description of all materials.

The base material is produced within a material vessel such that it forms a homogeneous, isotropic, and well-connected grain assembly with a specified non-zero material pressure using the material-genesis procedure that is defined in Potyondy and Cundall (2004) and extended in Potyondy (2014). The material-genesis procedure consists of a packing phase followed by a finalization phase. Each material is defined by a set of material properties. These properties control the material-genesis procedure, install the desired contact model at selected contacts, and assign contact-model properties. The base material of mixed-shape grains has a well-connected, but relatively loose, packing as compared with the more interlocked packing produced by the stamping logic of Cho et al. (2007), who refer to the resulting material as a clumped particle model and which we categorize as a clumped material.

A parallel-bonded material is a granular assembly in which the linear parallel bond contact model exists at all grain–grain contacts at the end of the material-finalization
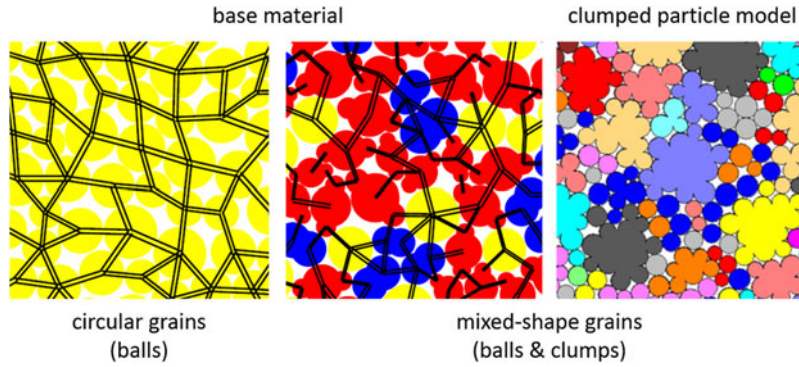
Figure 6. (Colour online) BPM base material consisting of grains (with balls in yellow and clumps in blue and red) and cement (drawn as pairs of black lines). An alternative clumped material is provided by the clumped particle model with grains outlined in black and assigned random colors and cement not shown. The image of the clumped particle model is from Figure 3(d) of Yoon et al. (2012).

phase, but only those grain–grain contacts with a gap less than or equal to the installation gap are bonded; new grain–grain contacts that may form during subsequent motion are assigned the linear contact model [which corresponds with the model of Cundall and Strack (1979)]. A parallel-bonded material mimics the microstructure of glass beads cemented with epoxy. A behavior summary of the linear parallel bond contact model follows – see Itasca Consulting Group, Inc (2014a) for a comprehensive description of the model.

The linear parallel bond contact model provides the behavior of two interfaces: an infinitesimal, linear elastic (no-tension), and frictional interface that carries a force and a finite-size, linear elastic, and bonded interface that carries a force and moment (see Figure 7). The first interface is equivalent to the linear model: it does not resist relative rotation, and slip is accommodated by imposing a Coulomb limit on the shear force. The second interface is called a parallel bond, because when bonded, it acts in parallel with the first interface. When the second interface is bonded, it resists relative rotation, and its behavior is linear elastic until the strength limit is exceeded and the bond breaks making it unbonded. When the second interface is unbonded, it carries no load.

A flat-jointed material is a granular assembly in which the flat-joint contact model exists at all grain–grain contacts with a gap less than or equal to the installation gap at the end of the material-finalization phase; all other grain–grain contacts as well as new grain–grain contacts that may form during subsequent motion are assigned the linear contact model. A flat-jointed material mimics the microstructure of angular, interlocked grains (similar to the marble shown in Figure 1). A behavior summary of the flat-joint contact model follows – see Itasca Consulting Group, Inc (2014a) for a comprehensive description of the model.

The flat-joint contact model provides the macroscopic behavior of a finite-size, linear elastic, and either bonded or frictional interface that may sustain partial damage. The interface is discretized into elements. Each element is either bonded or unbonded, and the breakage of each bonded element contributes partial damage to the interface. The behavior of a bonded element is linear elastic until the strength limit is exceeded and the bond breaks making the element unbonded, while the behavior of an unbonded element is linear elastic and frictional with slip accommodated by imposing a Coulomb limit on the shear force. Each element carries a force and moment that obey
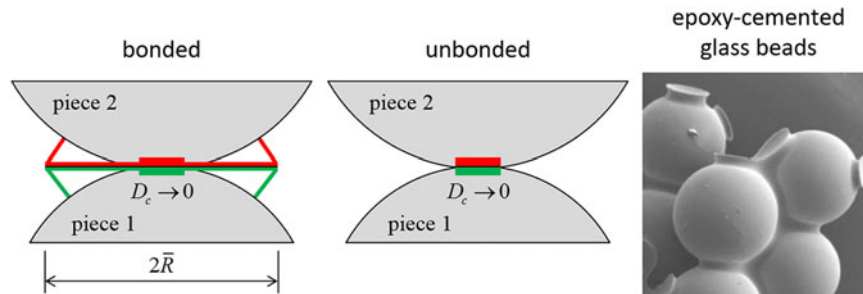

Figure 7. Parallel-bonded contact before (left) and after (middle) bond breakage. After the bond breaks, it is removed and the contact no longer resists relative rotation. A parallel-bonded contact that is bonded corresponds with a flat-joint contact that has all of its elements bonded. The image of epoxy-cemented glass beads is from Figure 4 of Holt et al. (2005).
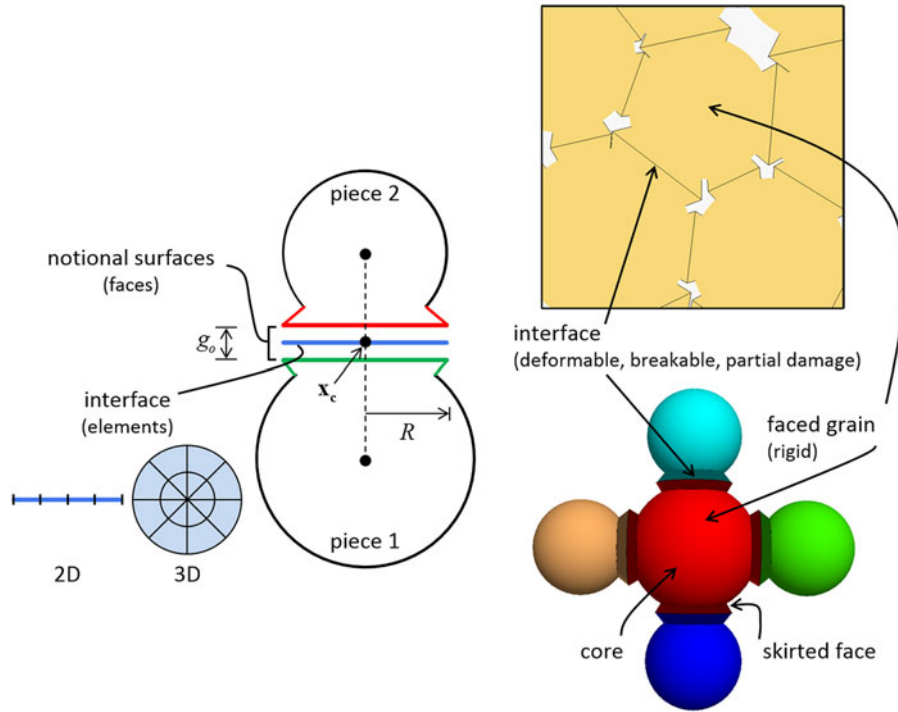
Figure 8.   Flat-joint contact (left) and flat-jointed material (right).

relatively simple force–displacement laws, while the force–displacement response of the flat-joint interface is an emergent behavior that includes evolving from a fully bonded state to a fully unbonded and frictional state.

A flat-joint contact and its corresponding flat-jointed material are shown in Figure 8. A flat-joint contact simulates the behavior of an interface between two notional surfaces, each of which is connected rigidly to a piece of a body. A flat-jointed material consists of bodies (balls, clumps, or walls) joined by flat-joint contacts such that the effective surface of each body is defined by the notional surfaces of its pieces, which interact at each flat-joint contact with the notional surface of the contacting piece. The notional surfaces are called faces, which are lines in 2D and disks in 3D. We refer to the balls of a flat-jointed material as faced grains, each of which is depicted as a circular or spherical core and a number of skirted faces. The faced grains are created when the flat-joint contact model is installed at the ball–ball contacts of a packed ball assembly. An interface exists between each set of adjoining faces and is discretized into elements with each element being either bonded or unbonded. The breakage of each bonded element contributes partial damage to the interface, and each breakage event is denoted as a crack (see Figure 9). If the relative displacement at a flat-joint contact becomes larger than the flat-joint diameter, then the adjoining faces may be removed (because the contact may be deleted) making the associated balls locally circular or spherical; if these balls

come back into contact, the behavior will be that of an interface between circular or spherical surfaces (if the linear contact model is assigned to the new contact).

Joints can be added to the base material using the smooth-joint logic (Itasca Consulting Group, Inc, 2014a; Mas Ivars et al., 2008) by which each joint is associated with an interface consisting of a collection of smooth-joint contacts between grains upon opposite sides of the joint. The smooth-joint contact model simulates the behavior of an interface, regardless of contact orientations along the interface by effectively modifying the surfaces of the contacting grains to align with the interface (see Figure 10).

3.4.   *Microstructural models provided by the BPM*

A rich variety of microstructural models can be produced with the BPM when it is viewed as a base material to which joints can be added. We first describe the sorts of microstructures that can be produced by modifying the base material itself. We then describe the larger-scale structural features (voids, material regions and joints) that can be overlaid on the base material and the types of models that can be produced. The focus in this section is on the microstructural and larger-scale features of these models.

The base material itself can serve as a model of intact rock. The base material produced by the material-genesis procedure of Potyondy and Cundall (2004) is an isotropic
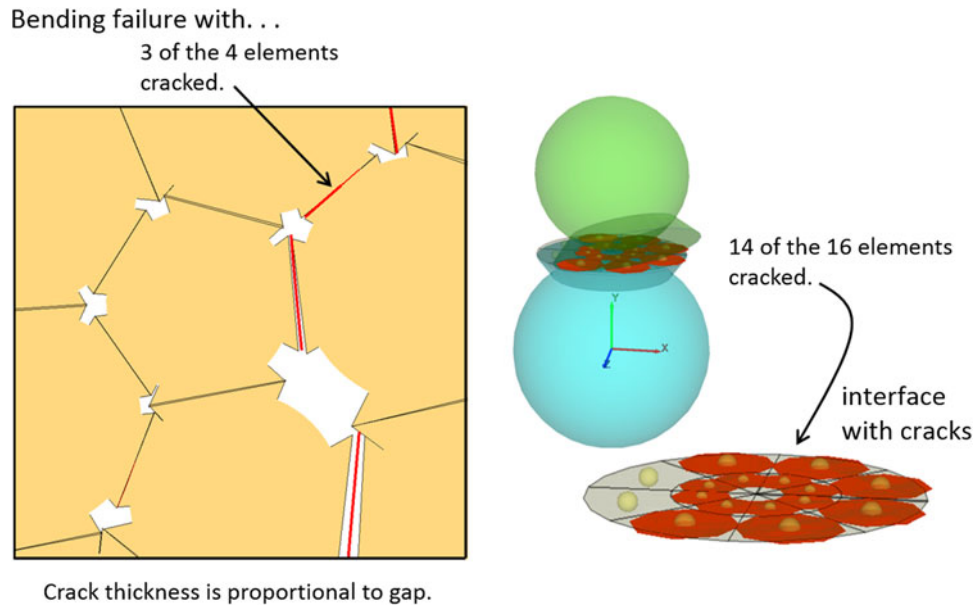
Figure 9.   (Colour online) Partially damaged flat-jointed material showing faced grains with cracks colored red/blue for tensile/shear failure.

and well-connected assembly of rigid grains joined by deformable and breakable cement that approximates the microstructure of an intact compact rock. The material is analogous to a brittle cookie dough that has been solidified by baking and for which grain size corresponds with dough granularity. The granularity is quantified by means of its resolution (or number of grains across a relevant dimension). The material is also analogous to intact rock which, as suggested in Section 2, can be viewed as an aggregate of crystals and amorphous particles joined by varying amounts of cementing materials. This base material approximates an intact compact rock with average homogeneous isotropic properties at a scale larger than the material granularity.

A rich variety of microstructures can be produced by modifying the base material itself. Such microstructures are obtained either by modifying the properties of the grains and cement or by modifying the packing fabric. The grain properties are size and shape. The cement properties are deformability and strength as well as evolving damage (e.g., as provided by the flat-joint contact model and which contributes to match the uniaxial and tensile strengths of compact rock – see Section 4.2). The cement properties are embodied in the contact model, but the macroscopic material behavior is also sensitive to the ways in which new contacts form and contacts deemed to be broken behave. The packing fabric is affected by the size distribution and shapes of the grains as well as the material-genesis procedure. For example, the material-genesis procedure could be modified to produce an anisotropic and less well-connected fabric by compacting the grains under gravity loading with high friction.

Structural features at a scale larger than the material granularity can be overlaid on the base material. These features include voids, material regions, and joints. In addition, grain-based models combine material regions and joints.
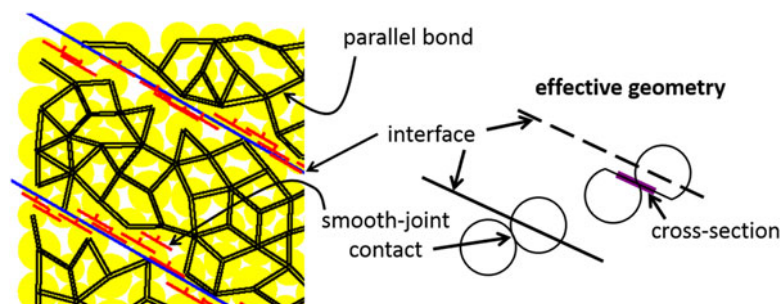

Figure 10.   (Colour online) A pair of joints overlaid on a parallel-bonded base material (with balls in yellow, interfaces in blue, smooth-joint contacts in red, and remaining parallel bonds drawn as pairs of black lines). The effective interface geometry is shown on the right.
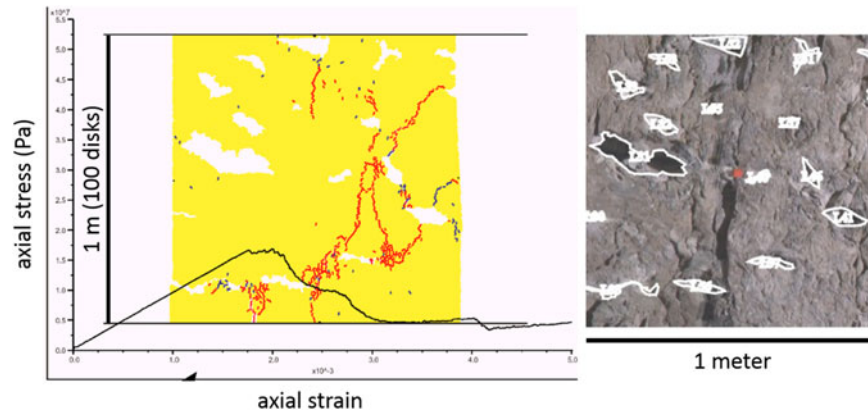
Figure 11.   (Colour online) Damaged BPM in the post-peak stage of an unconfined-compression test and corresponding panel map of the Cross-Drift tunnel through the lithophysal rock unit at Yucca Mountain (Potyondy, 2007b). The identified structural features are lithophysal cavities, spots, and lithic clasts. Bond breakages (red/blue for tensile/shear breakage) nucleate at void boundaries and coalesce into macroscopic fractures. The specimen continues to carry load because of load redistribution among uncracked material regions. This process is evident in Figure 3 where much of the load is being carried within the specimen center.

3.4.1.   Void regions

Void regions are identified, and the grains that lie within these regions are deleted. Examples of BPMs that contain void regions are shown in Figures 3 and 11.

3.4.2.   Material regions

Material regions are identified, and the grains and contacts that lie within these regions are assigned the corresponding material properties. Each grain is mapped into a single material region. Each contact is either mapped into a single material region, or the contacts that lie along the region boundaries are identified and assigned interfacial properties. An example of a BPM that contains different material regions is shown in Figure 12. The adjoining surfaces of interfaces defined by the contacts that lie along the region boundaries appear bumpy at the scale of the grains, and the mechanical behavior will reflect these granular asperities. The model shown in Figure 12 exhibits this behavior. If such spurious asperity interlock is of concern, then it may be possible to remove this effect by assigning the smooth-joint contact model to these contacts, and this presents a promising avenue for further study.

The clumped particle model shown in Figure 6 can also be included in the present category. In this case, the material regions are identified as arbitrarily overlapping circular stamps that are applied sequentially. The grains (circular balls in this case) within each stamp are identified and transformed into the pebbles of a clump. If a stamp contains balls that have already become pebbles, then these balls are reassigned to the new clump associated with that stamp. The microstructure produced by this procedure is highly interlocked and approximates the microstructure of an intact igneous rock consisting of a crystalline assemblage of minerals. It is more interlocked than the
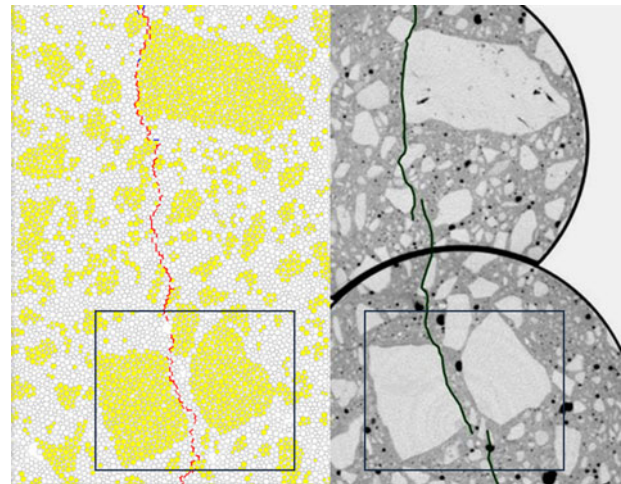

Figure 12.   Damaged BPM and corresponding computer tomography image of concrete with large coarse aggregates [from Figure 6 – 3 of Katsaga (2010)]. Microstructural features of the concrete are matrix material, aggregates, and matrix–aggregate interfaces. The BPM base material represents the matrix material, and the aggregates and interfaces are identified by overlaying the CT image on the base material. The macroscopic fracture identified in the BPM as the coalescence of broken bonds is similar to the macroscopic fracture identified in the CT image.

microstructure shown in the middle image of Figure 6, which results from a material-genesis process in which the grains (which may be clumps of complex shape) are made frictionless and compacted at a specified confining pressure. A promising avenue for further study would be to examine the differences in the macroscopic response of materials with these two differing microstructures, and also to consider other highly interlocked microstructures such as the particle clusters shown in Figure 11 of Potyondy and

Cundall (2004). Such study would enhance our understanding of the relevant microstructural attributes of a BPM for intact compact rock and would also contribute to the development of a BPM for intact porous rock.

3.4.3. Joints

Joints are identified, and the contacts that lie along these joints are assigned the corresponding joint properties. The joints are added sequentially. The contacts between grains upon opposite sides of the joint are identified, and the contact model of each of these contacts is replaced by the smooth-joint contact model. When each joint is added, contacts that have been assigned to a previous joint are ignored giving a precedence to the joint-insertion process. The joints can overlap one another and need not enclose separate material regions (i.e., the joints need not define separate blocks of material like those shown in Figure 1, instead they may terminate within blocks). The BPMs produced by this process can be remarkably complex as shown in Figure 13. Such BPMs combine the microstructural features of intact rock with a larger-scale joint fabric to provide a Synthetic Rock Mass that has been used to obtain a better understanding of the joint fabric and its impact on rock mass strength, brittleness, and fragmentation (Mas Ivars et al., 2011). A simpler example of a BPM with joints is given in Section 4.1.

3.4.4. Grain-based models (GBMs)

Two-dimensional grain-based models provide a synthetic material that mimics deformable, breakable polygonal grains with deformable, breakable grain–grain interfaces.

Such models are constructed by overlaying a polygonal grain structure on the base material and representing the interfaces via smooth-joint contacts. GBMs combine the material regions and joints described earlier. The grain structure is a polygonal mesh that completely fills space: there are no gaps between polygons – each polygon edge is either internal (adjacent to two polygons) or external (adjacent to one polygon) such that each polygon and internal edge correspond with a grain and a grain–grain interface, respectively (see Figure 14). Material properties are associated with the grains and the interfaces such that both entities are deformable and capable of fracturing. Grains mimic a cemented granular material, and interfaces mimic a cemented joint; in both cases, the cement is represented by bonds that join two opposing particle surfaces. Grain fracture occurs when the internal bonds break, and interface fracture occurs when the bonds along the interface break. As more bonds break, the grain behavior approaches that of a granular material with frictional sliding at particle–particle contacts, and the interface behavior approaches that of a joint obeying Coulomb sliding with dilation. The grain-based modeling procedure is described in Potyondy (2010b).

An ideal grain structure should have topological and statistical properties similar to those of real rock. Voronoi tessellation is often used to generate polycrystalline microstructures, but the topological and statistical properties of such structures differ from real polycrystalline assemblies and a size-distributed, sphere-packing scheme gives a better match (Zöllner, 2006). A disk-packing scheme (illustrated in Figure 15 and described in Potyondy (2010c)) has been developed and used to produce the grain
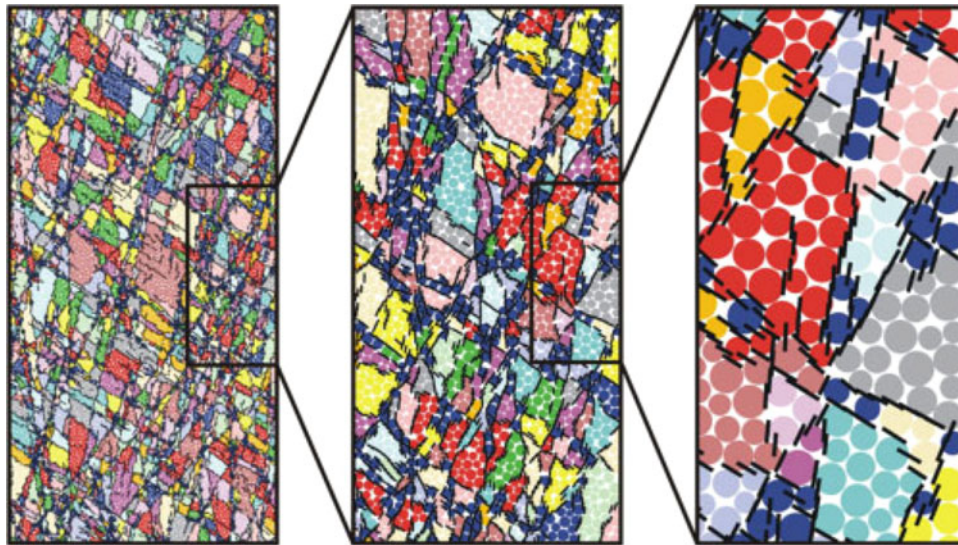

Figure 13.   (Colour online) A 2D Synthetic Rock Mass [from Figure 2 of Pierce and Fairhurst (2012)]. The smooth-joint contacts are drawn as short black lines, and the grains of the BPM base material are colored to denote blocks. Each block is defined as the set of grains that can be reached by traversing intact parallel bonds. A relatively small set of colors is used so that some adjacent blocks share the same color. As the parallel bonds break in response to macroscopic loading, the blocks break into smaller blocks (or fragments).
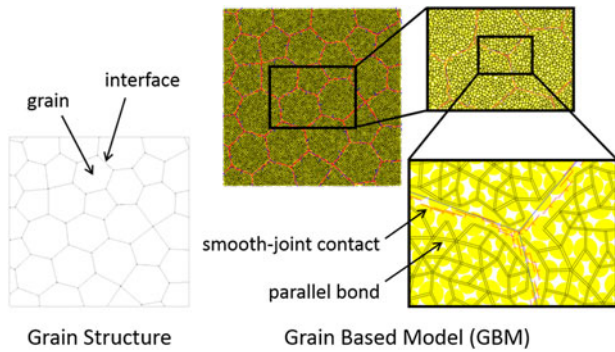
Figure 14. (Colour online) Grain structure consisting of polygonal grains separated by interfaces and grain-based model consisting of grains and interfaces. The grain structure is overlaid on a parallel-bonded base material (with balls in yellow, smooth-joint contacts in red, and remaining parallel bonds drawn as pairs of black lines).

structures of the models described in Section 4.2. The topological and statistical properties of the structures produced by this scheme have not been compared with those of real rock. A promising avenue for further study would be to compare the properties of these alternative structures and determine their effect on the behavior of GBMs.

4. Examples

The following three examples demonstrate how BPMs are used to model rock at both an intact and rock-mass scale. The first example describes an intact anisotropic material that may swell and contract in response to changes in saturation, and demonstrates how the macroscopic behavior of this material arises from its microstructural features. The second example explores the behavior of two alternative intact BPMs that can match both the uniaxial and tensile strengths of compact rock. The microstructural features required to match these strengths are discussed, and the direct-tension and compression-test response of these two materials are compared with the expected

response of compact rock. The third example describes how an intact BPM can be embedded within a larger continuum model to study the fracturing around a stope in quartzite. It is demonstrated that damage can occur within both material idealizations (continuum and discrete) and propagate across the coupling boundary with minimal disturbance.

4.1. Anisotropic material that may swell and contract in response to changes in saturation

A bonded-particle model has been developed to study the fracturing processes and time evolution of excavation damage zones in argillaceous materials, with particular focus on explaining the processes occurring at the Tournemire site (Rejeb & Cabrera, 2006). The following mechanisms may be relevant: (1) the material possesses an anisotropic fabric consisting of bedding planes, and discrete fractures may form in the material both within and across the bedding planes; (2) the material experiences internal mechanical suction arising from capillary pressure, and changes in saturation may damage the material; and (3) the material flows in response to sustained stress, exhibiting a creep-like behavior. An ideal model would provide all of these mechanisms. The current model provides the first two mechanisms by: (1) adding parallel interfaces at a fixed spacing to the BPM base material produced by the material-genesis procedure of Potyondy and Cundall (2004) and (2) adding capillary pressure-induced suction forces at the grain–grain contacts of the BPM base material – the capillary pressures are linked to the saturation via two-phase flow theory, which provides a relation between saturation and effective pressure within the material. The model behavior is summarized here – see Potyondy and Emam (2008, 2009) for a complete description.

The synthetic material exhibits transversely isotropic material behavior and reproduces the primary damage mechanisms of desiccating clay. The material matches the unconfined-compression test response (variation with loading angle of effective Young's modulus and
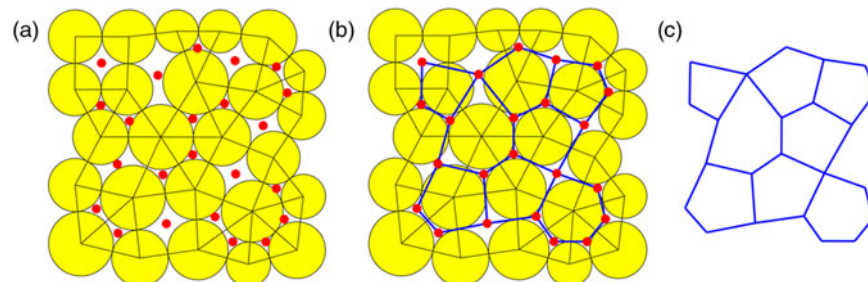

Figure 15. Disk-packing scheme. Initial disk packing showing disks and contacts with filled circles at internal-void centroids in (a). Generated grain structure consisting of polygons, one for each internal disk, with nodes at internal-void centroids in (b) and final grain structure in (c).

compressive strength) of fully saturated argillite specimens and the free uniform drying response (volumetric strain versus saturation) of a partially saturated argillite specimen.

Unconfined-compression tests are performed on 1-m square specimens with parallel interfaces at 10-cm spacing, and results from these tests are compared with laboratory results obtained from much smaller argillite specimens (see Figures 16 and 17 in which the loading angle is defined as the smallest angle between the loading direction and the bedding planes such that a loading angle

of 90° corresponds with loading perpendicular to the bedding). The stress–strain curves are approximately linear, with a well-defined peak followed by an abrupt loss of strength, exhibiting a brittle post-peak response. The effective modulus and peak strength vary with loading angle and reflect the material anisotropy. We offer the following micromechanical explanations for these variations.

- The interfaces are softer than the layers. For a loading angle of zero, all of the load is carried in the
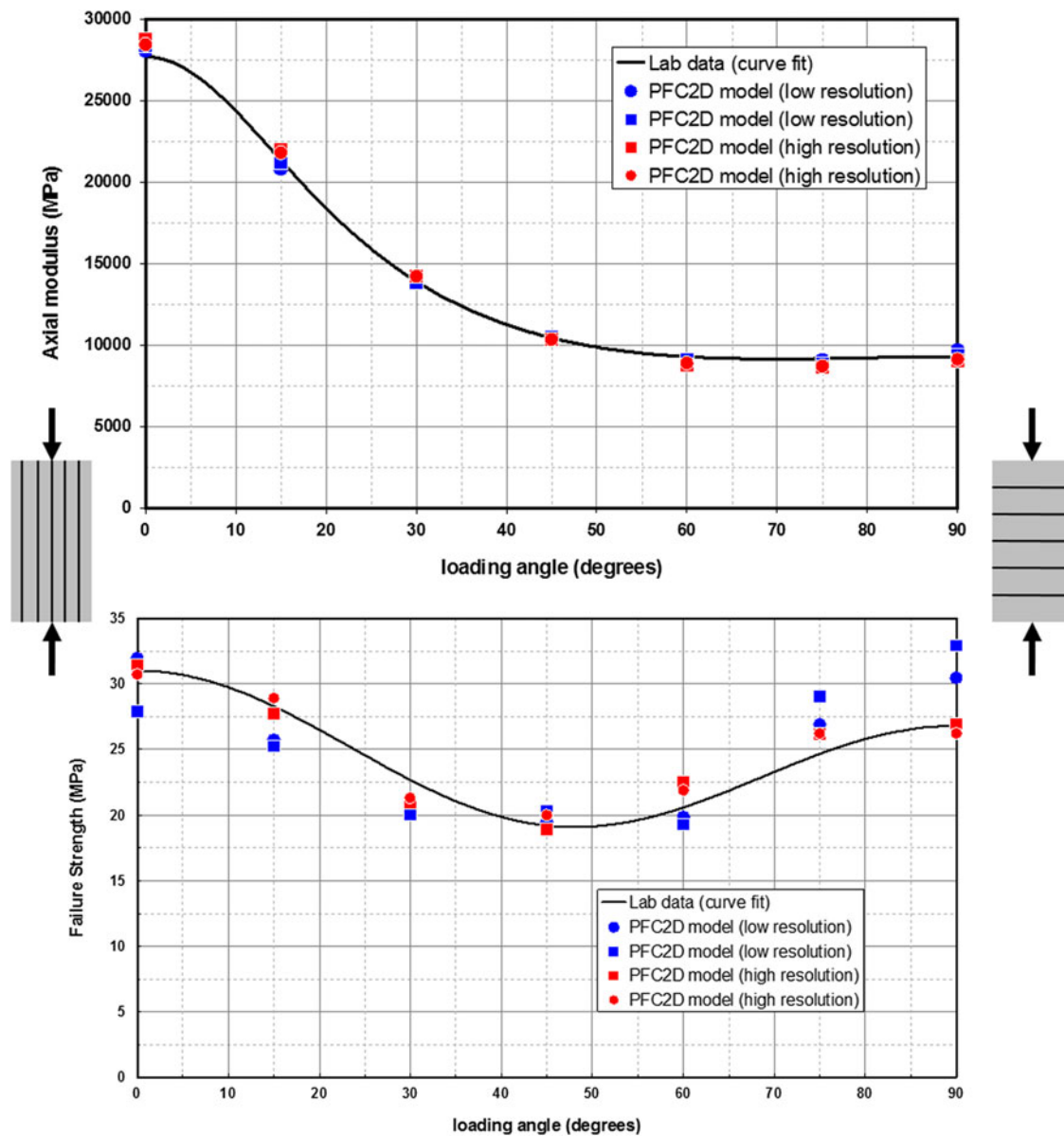

Figure 16. Effective modulus (above) and peak strength (below) versus loading angle of argillite specimens. The curve denoted as "Lab data (curve fit)" in the effective-modulus plot is for a transversely isotropic material model whose constants have been chosen to match the laboratory data. The low- and high-resolution materials have 4 and 8 grains, respectively, across each layer. The low-resolution material is shown in Figure 10. The circles and squares in the legend denote responses for two instances of each material that differ only in their packing arrangements.
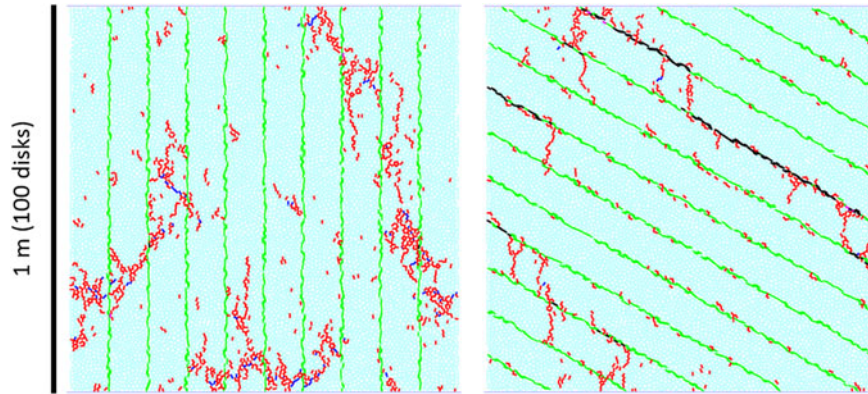
Figure 17. (Colour online) Damage (bond breakages in red/blue for layer tensile/shear failure and magenta/black for interface tensile/shear failure) at post-peak stage of unconfined-compression tests on argillite specimens (parallel bonds in light cyan and smooth-joint contacts in green) at loading angles of 0° (left) and 60° (right).

stiffer layers, and thus this orientation has the largest effective modulus. As the loading angle increases, an increasing portion of the load is carried in the softer interfaces, and thus the effective modulus decreases.

• The interfaces are weaker than the layers. For loading angles of 0° and 90°, the peak stress coincides with damage localizing in the layers, and thus peak strength is controlled by layer strength. For loading angles from 30° to 60°, the peak stress coincides with damage localizing in a single interface and then bridging between the interfaces, and thus the peak strength is controlled by interface strength.

The primary damage mechanisms of desiccating clay are summarized as follows (Costa, Kodikara, & Thusyanthan, 2008). Material drying induces suction loading that forces the material to contract. Significant tensile forces can develop at the boundaries of the contracting regions. These boundaries may be the specimen boundaries or the tip of an internal fracture over which suction does not act. When the BPM base material with suction forces at grain–grain contacts is subjected to a fully constrained drying test whereby a fully saturated specimen has its uniform saturation gradually reduced, then cell-like structures comprised of 10–20 grains form, with the cell interiors in compression and the cell boundaries in tension. Fractures nucleate along some of the cell boundaries when saturation reaches 0.97 (see the left-most image in Figure 18). When the saturation is reduced to 0.96, these fractures grow and break the specimen into isolated blocks, each of which contracts toward its center. No suction acts across each broken grain–grain contact; thus, the fracture tips are subjected to an opening mode of loading that induces continued fracture growth from each tip. The final fracture pattern is analogous to desiccation cracking in clay. A promising avenue for further study would be to continue the development of the BPM described in this section. Such
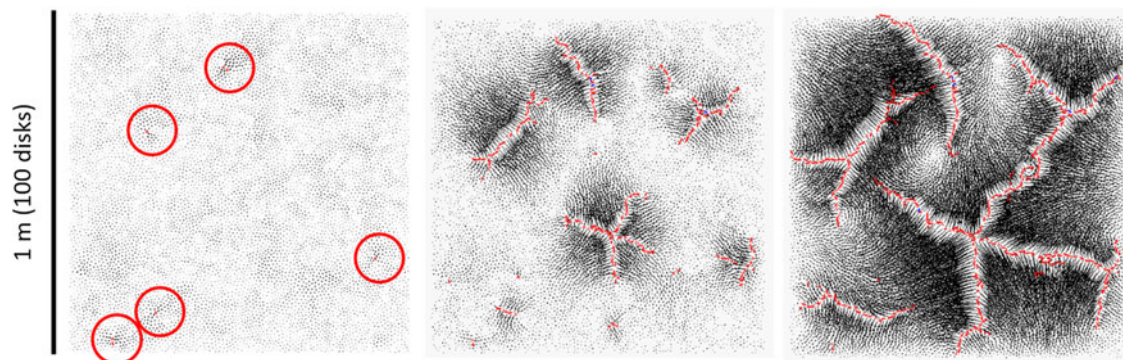

Figure 18. Damage development (bond breakages in red/blue for tensile/shear failure) in BPM with suction. The specimen is subjected to fully constrained uniform drying to saturation of 0.97 in left-most image (with broken bonds circled), and 0.96 in the remaining two images. The drying-induced displacement field is depicted as black arrows emanating from each grain of the BPM base material.

study would enhance our understanding of the progressive weakening of argillaceous materials that swell and contract in response to changes in saturation.

4.2. Matching both the uniaxial and tensile strengths of a typical compact rock

A BPM consisting of parallel-bonded disks or spheres suffers from the limitation that if one matches the unconfined-compressive strength (q_u) of a typical compact rock, then the direct-tension strength (σ_t) of the model will be too large. This limitation can be overcome by introducing intergranular interlock in the form of a well-connected grain structure with interfaces that are deformable, breakable, and capable of sustaining partial damage by evolving from a fully bonded state to a fully unbonded and frictional state that continues to resist relative rotation. Partial interface damage with continued moment-resisting ability is an important microstructural feature of a BPM. Both the 2D grain-based and flat-jointed materials provide such a grain structure (see Figure 19) and, thus, overcome this limitation.

Why is it that the flat-jointed material can match the relatively large (q_u/σ_t) ratio of a typical compact rock, but the parallel-bonded material cannot? During an unconfined-compression test on a parallel-bonded material with its tensile strength chosen to match σ_t and its shear strength infinite, failure at peak load is triggered by disk rolling arising from a lack of moment resistance after bond failure – the peak load is much lower than that of a typical compact rock and cannot be increased because its shear strength is already infinite. The corresponding flat-jointed material has its tensile strength chosen to match σ_t and exhibits continued moment-resisting capacity after partial damage forms in an unconfined-compression test – the peak load is controlled by its shear strength, which can be chosen to match q_u (Potyondy, 2012).

Two-dimensional GBMs with unbreakable grains can also be simulated using Voronoi blocks within the program UDEC (Itasca Consulting Group, Inc, 2014b). UDEC GBMs have been used to study damage processes occurring in a laboratory specimen subjected to compressive loading (Lan, Martin, & Hu, 2010) and in the rock around a tunnel (Damjanac, Board, Lin, Kicker, & Leem, 2007). Both UDEC GBMs and the GBMs described here have been used to study spalling in hard rock (Potyondy, 2009; Potyondy, Cundall, DeGagne, & Corkum, 2008; Potyondy, Ekneligoda, & Fälth, 2009). For the case of unbreakable grains, the 2D flat-jointed material is less computationally demanding than either of these alternative GBMs.

The compressive behavior of the 2D grain-based and flat-jointed materials described in the two subsections below is similar to that of granite as summarized in Section 2.1. The main discrepancy is the lack of transgranular microcracking in the synthetic materials. In granite, such microcracking commences after the crack-initiation point and accelerates with increasing load such that at peak stress, nearly all grains contain new transgranular fractures. Transgranular microcracking can be allowed to occur in the 2D grain-based material by specifying realistic grain microstrengths – the grain microstrengths were made infinite in the material described below. Allowing the grains to break may produce volumetric-strain reversal before peak load. It has also been found that a 2D grain-based material with unbreakable grains does not match the Brazilian-test behavior of compact rock, because it does not exhibit a brittle load–displacement response; however, the response becomes brittle if the grains are allowed to break (Bahrani et al., 2012). A promising avenue for further study would be to explore the effects of grain breakage on BPM behavior.

We demonstrate in the following two subsections that the 2D grain-based and flat-jointed materials can match
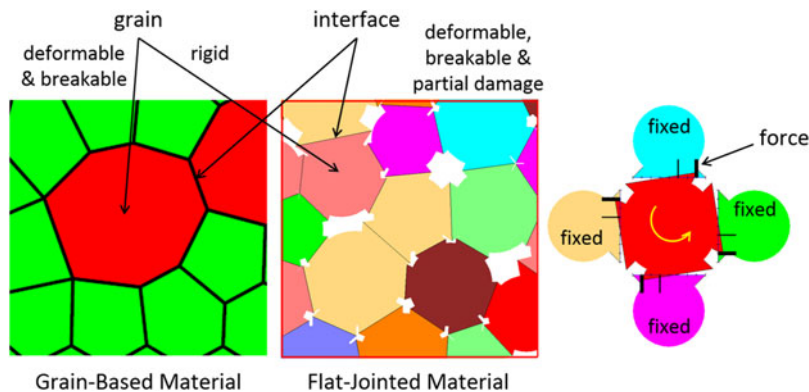

Figure 19. Grain structure and interfaces of 2D grain-based and flat-jointed materials of intact compact rock (left and middle) as well as interlocked grain modeled with four fully unbonded flat-joint contacts (right). Compressive forces develop at the far end of each flat-jointed interface to resist the moment applied to the central grain so that even the fully unbonded interface continues to resist relative rotation.

most of the primary features, both qualitative and quantitative, of a typical compact rock (taken here to be Äspö diorite for the 2D grain-based material and Castlegate sandstone for the 2D flat-jointed material) subjected to direct-tension and compression tests.

4.2.1. Grain-based material

The test responses of the 2D grain-based material with unbreakable grains are summarized as follow [see Figure 20 and Potyondy (2010d)].

- *Direct-tension test response.* The measured property (σ_t) matches that of Äspö diorite. The material response is brittle with an abrupt drop in load after peak. Damage begins near peak load, and consists of a sparse collection of homogeneously distributed interface tensile breaks predominantly oriented perpendicular to the loading axis. At peak load, damage begins to localize at a few of these sites and eventually forms fractures that follow the grain boundaries and traverse across the specimen. All breaks are interface tensile breaks, and the resulting damage surfaces follow the grain boundaries, producing rough rupture surfaces.

- *Unconfined-compression test response.* The measured properties match those of Äspö diorite, with the exception that the Poisson's ratio is underestimated and volumetric-strain reversal does not occur before peak load. Interface tensile breaks begin to form at a low axial load but do not reach a sufficient density to cause the lateral versus axial strain curve to deviate markedly from linearity until the crack-initiation point. At this point, there are no interface shear breaks, and the interface tensile breaks are distributed homogeneously throughout the specimen with most being aligned subparallel to the loading axis. As loading proceeds, more interface tensile breaks form and begin to coalesce along entire grain edges, but typically do not link together between adjacent grain edges until significant numbers of interface shear breaks also have formed (at just before peak load). The interface shear breaks contribute to the formation of fractures that are aligned subparallel to the loading axis and span multiple grains. As these fractures open, they appear as unloading regions in force-chain plots. Many of these fractures form at peak load and break the material into multiple interlocking columns; the
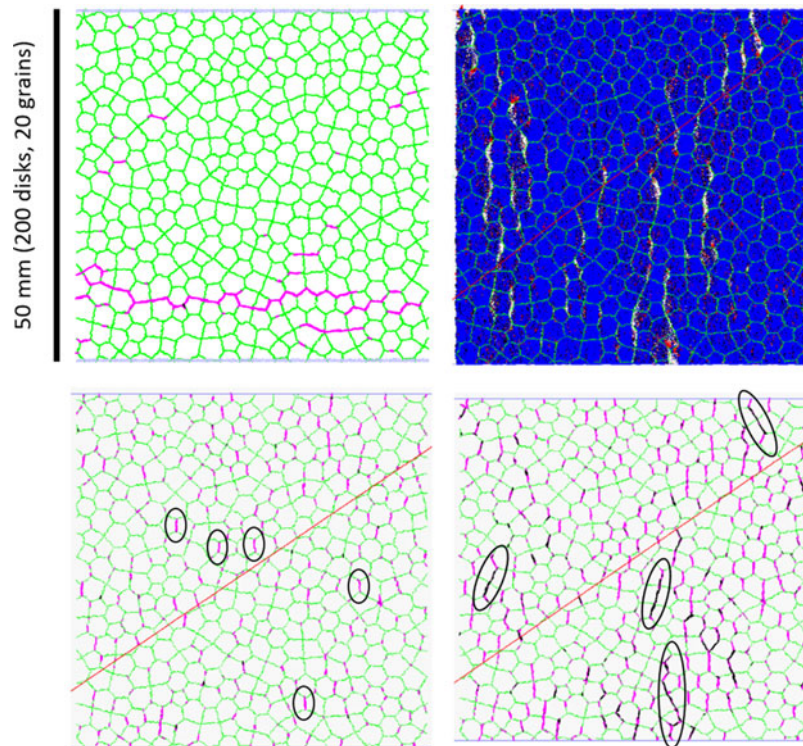

Figure 20. Damage development in 2D grain-based material with unbreakable grains. Damage at final post-peak load of direct-tension test (top left) and unconfined-compression test (top right). Damage during unconfined-compression test at half-way point (bottom left – some fully cracked grain edges are circled) and peak load (bottom right – some adjacent fully cracked grain edges that have failed predominantly in shear are circled). Smooth-joint contacts are green, breakage modes are magenta/black for interface tensile/shear failure and force chains are blue for disk-disk compression and black/red for compression/tension in parallel bonds. Diagonal lines in the compression-test images are to be ignored.

behavior is similar to axial splitting. The formation of these columns induces significant dilation and produces volumetric-strain reversal. These fractures are similar to spalls, because their surfaces experience purely opening-mode displacements after they form – i.e., there is no grinding together of the new surfaces; instead, they split apart and form a gap. There is no load carried across such a gap, which is why it appears as an unloading region in a force-chain plot.

4.2.2.   Flat-jointed material

The test responses of the 2D flat-jointed material are summarized as follow [see Potyondy and Xiao (2014) and note that the 3D flat-jointed material exhibits similar behavior (Potyondy, 2014)].

- *Direct-tension test response.* The measured property (σ_t) matches that of Castlegate sandstone. Very little cracking occurs until just before the peak stress is reached. Peak stress coincides with the formation of a few tensile fractures aligned perpendicular to the specimen axis. Damage in each tensile fracture consists of perpendicularly oriented tensile cracks. Formation of the tensile fractures produces a brittle stress–strain curve with no residual strength.
- *Unconfined-compression test response.* The measured property (q_u) matches that of Castlegate sandstone. Substantial cracking is evident before the peak stress is reached. The cracks are distributed throughout the specimen with most of them being parallel to the specimen axis, and almost all cracks

are tensile. Peak stress coincides with axial splitting during which the material breaks apart into multiple interlocking axial columns. The axial splitting produces a brittle stress–strain curve with no residual strength. Damage at the post-peak state is described as follow (see Figure 21): almost all cracks are tensile and aligned with the specimen axis, many of the cracks are dilating and some interfaces have partial damage and are subjected to bending.

- *Confined-compression test response.* Before peak stress, damage consists of uniformly distributed tensile cracks aligned parallel with the specimen axis, and peak stress coincides with the formation of a few diagonally aligned shear fractures. The stress drops during the formation of these shear fractures and reaches a non-zero residual value after they have formed. The damage differs outside of and within the shear fractures (see Figure 21). Outside of the shear fractures, the damage is similar to that in an unconfined-compression test. Within a shear fracture, the cracks are both tensile and shear, and most are aligned with the specimen axis. There is extensive dilation in which many of the cracks have opened and grains have repacked into a less dense state; the cracks outside of the shear fractures are much less dilated.
- *Fragmentation.* Fragmentation during compression tests is shown in Figure 22. The fragmentation is sensitive to confinement and becomes extensive with the application of sufficient axial strain. For unconfined conditions, fragmentation consists of axially aligned columns with extensive dilation
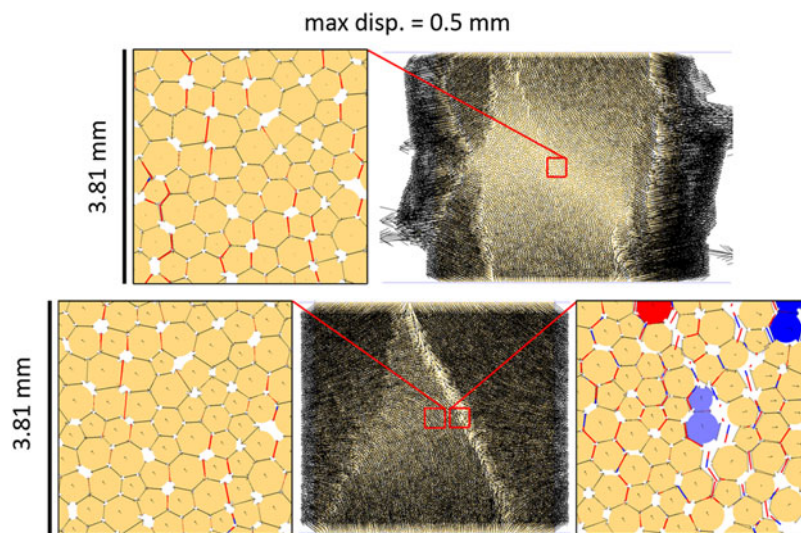

Figure 21.   Damaged microstructure of 2D flat-jointed material at post-peak stage of compression tests. The damage in the unconfined test (top) is characterized by axial splitting, whereas the damage in the confined test (bottom) is charactered by the formation of a few diagonally aligned shear fractures.
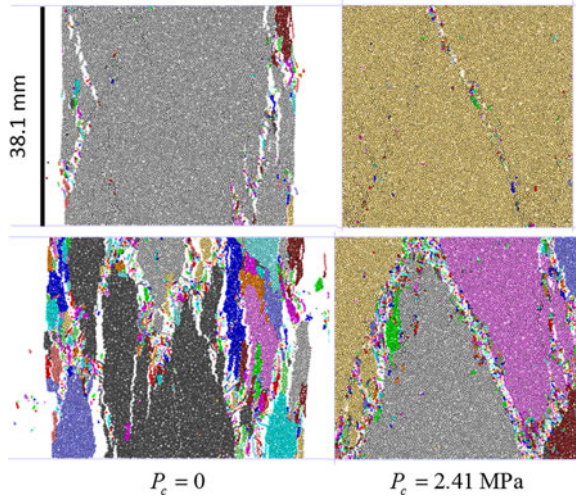
Figure 22. Fragmentation of 2D flat-jointed material at post-peak (top) and residual (bottom) stages of compression tests. A fragment is defined as a set of grains joined by flat-joint contacts that have at least one of their elements bonded, and fragments are depicted by grain color.

between the columns. For confined conditions, fragmentation is controlled by the shear fractures which delineate a few large fragments with extensively dilated comminuted material (comprised of much smaller fragments) between the large fragments.

4.3. *Fracturing around an advancing stope in quartzite*

A coupled continuum-discontinuum model has been developed to study the fracturing that occurs around an advancing stope in quartzite. The coupled model embeds a BPM for intact rock within a larger continuum FLAC (Itasca Consulting Group, Inc, 2011) model. The coupled model demonstrates how the BPM can be used to simulate boundary-value problems at a scale that appears in engineering and mining work. When applying the BPM to such problems, we make the grains much larger than the real grains, and must then consider the synthetic material to be an analog material intended to capture the relevant microbehavior. The material is first calibrated to match laboratory-scale response of intact rock, and then the material microproperties are degraded to account for scale effects that cause the *in situ* rock strength to be less than the intact rock strength. A promising avenue for further study would be to explore how best to incorporate scale effects into the BPM material, and thereby either replace or justify the *ad hoc* strength-reduction schemes employed at present. The coupled model itself and its behavior are summarized here – see Katsaga and Potyondy (2012) for a complete description.

The stope excavation is idealized by assuming that the panel is long in the dip direction such that two-dimensional, plane-strain conditions are appropriate. The coupled model consists of a FLAC model within which is embedded a PFC2D inclusion (see Figure 23). The FLAC model is run under conditions of plane strain, and the PFC2D model behaves as an assembly of unit thickness rods; thus, conditions of plane stress or plane strain cannot be imposed. The FLAC model can be run in either small- or large-strain mode; the PFC2D model behaves similarly to a large-strain mode, because particle positions are updated. Both codes are set to approximate quasi-static conditions for which the model response is heavily damped. The initial model contains no stope, and
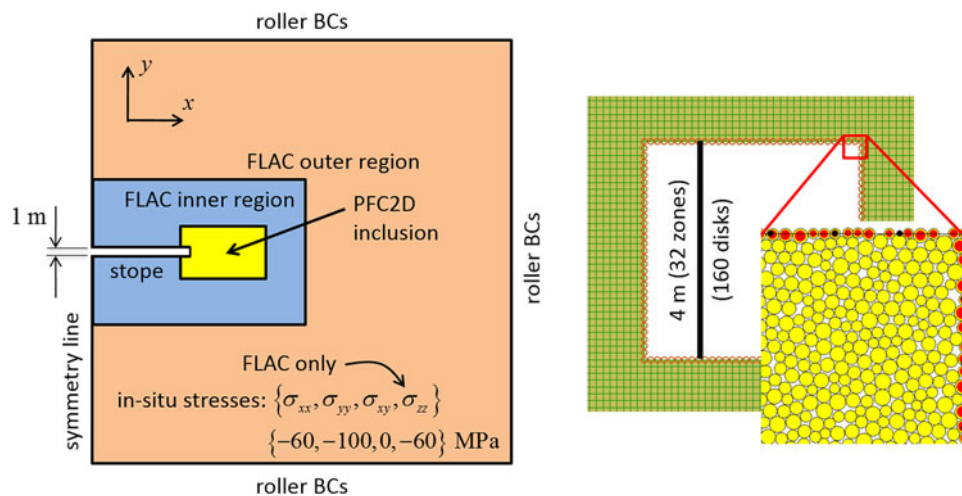

Figure 23. Sketch of coupled model (left) and PFC2D inclusion consisting of an enhanced parallel-bonded material (right). The inclusion boundary of the FLAC grid is drawn with open circles at each boundary grid point, boundary particles in the PFC2D inclusion are red and edges of FLAC boundary zones and gridpoints are black. The boundary particles are effectively slaved to move with the edges of the boundary zones – the coupling logic is described in Itasca Consulting Group, Inc (2008).
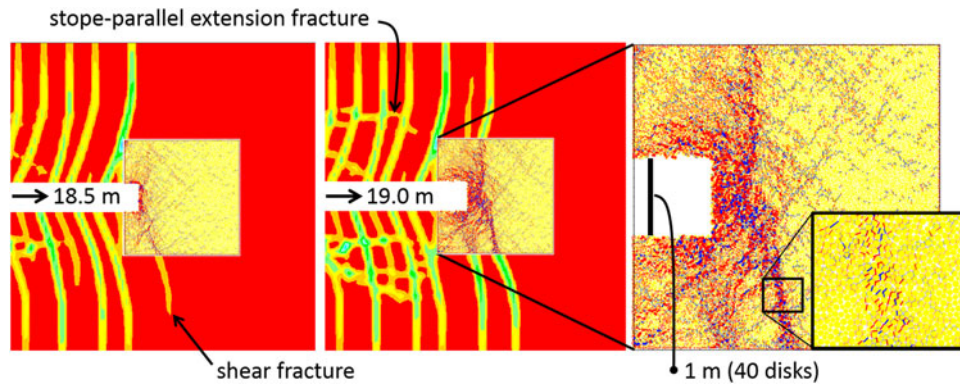
Figure 24. Fracture pattern in coupled model depicted as maximum shear strain in FLAC material (scaled to maximum of 0.05) and damage plot in PFC2D material (with red/blue for tensile/shear breakage and thickness proportional to the gap between previously bonded disks) at stope half-lengths of 18.5 and 19.0 m.

excavation proceeds from left to right starting at the line of symmetry.

In the FLAC model, the quartzite is modeled as a strain-hardening/softening material. The FLAC strain-hardening/softening material model allows representation of nonlinear material softening and hardening behavior based on prescribed variations of the Mohr–Coulomb model properties as functions of accumulated plastic strain. In the PFC2D model, the quartzite is modeled as an enhanced parallel-bonded material. Enhanced parallel bonds include a moment-contribution factor described in Potyondy (2011) that allows the PFC2D material to match both the uniaxial and tensile strengths of quartzite. The flat-jointed material did not yet exist at the time of this summarized work; it is expected that damage studies undertaken with any parallel-bonded BPM will benefit from use of the flat-jointed material. To account for scale effects that cause *in situ* rock strength to be less than intact rock strength, the material properties are chosen to match the intact strength of Maraisburg quartzite, and then the cohesion of both the FLAC and PFC2D materials is halved. Confidence in this *ad hoc* strength-reduction scheme was gained by modeling pillar behavior with the FLAC and PFC2D materials, and then comparing the responses with one another and with *in situ* pillar strength data. The pillar-modeling results suggest that the tensile strength of the PFC2D material also should be halved, which has been done to produce the results summarized here.

Fracture pattern is the main criterion used to judge the validity of the coupled model. The expected fracture pattern for a stope in homogeneous and isotropic quartzite with no parting planes consists of shear fractures that form ahead of the advancing face and stope-parallel extension fractures that form behind the face. The fracture pattern in the coupled model near the stope face is shown in Figure 24. This pattern compares well with the expected pattern. When the half-length of the stope is 18.5 m, a

shear fracture emanates from the stope face and extends into the footwall. After the stope extends by one-half meter, this shear fracture has grown and two new shear fractures have formed. These results demonstrate that damage can propagate across the coupling boundary with minimal disturbance. The PFC2D material reveals a richness of detail in its damage plots that is absent in the FLAC damage plots and includes significant distributed cracking ahead of the stope face as well as shear fractures that are identified as bands of dense cracking. By comparing the responses of these two different material idealizations, it may be possible to obtain a better understanding of the damage processes occurring around real stopes and within real shear fractures, and this presents a promising avenue for further study.

5. Conclusions

The bonded-particle modeling methodology supports the creation of a variety of microstructural models for rock. These models provide a wide range of rock behaviors that encompass both compact and porous rock at both an intact and rock-mass scale. The modeling of rock-mass behavior employs the Synthetic Rock Mass (SRM) approach which overlays a larger-scale joint fabric on the intact base material. A challenge for SRM modeling is the accurate reproduction of the joint fabric present in the real rock (Pierce & Fairhurst, 2012). SRM modeling will also benefit by improvements to the intact base material, because this will allow the rock blocks to fragment in a more realistic fashion. The following three paragraphs discuss our abilities to model intact rock in both two and three dimensions.

Intact compact rock in two dimensions can be modeled reasonably well using either 2D grain-based or 2D flat-jointed materials. Both of these materials match much of the response obtained during direct-tension and compression tests of a typical compact rock, including the

uniaxial and tensile strengths. The brittle failure behavior of granite in uniaxial compression that is summarized in Section 2.1 suggests that grain breakage is occurring before peak stress, and we postulate that this may be what causes the pre-peak volumetric-strain reversal (so that specimen volume begins to increase). It may be possible to match this behavior with a 2D grain-based material for which the grain structure has been overlaid on a 2D flat-jointed base material. The use of a 2D flat-jointed base material will allow the grains to have a high uniaxial to tensile strength ratio, if necessary.

Intact compact rock in three dimensions can be modeled using the enhanced parallel-bonded material that includes a moment-contribution factor (β) described in Potyondy ([2011](#)). Setting $\beta = 1$ recovers the standard parallel-bonded material, and setting $\beta = 0$ allows the uniaxial and tensile strengths of a typical compact rock to be matched. But the use of $\beta = 0$ is questionable, because it implies that forces contributing to the elastic bending response are ignored when considering bond failure. The 3D flat-jointed material provides a more mechanistically defensible model that matches much of the response obtained during direct-tension and compression tests of a typical compact rock, including the uniaxial and tensile strengths. If it is deemed necessary to allow for grain breakage, then a 3D grain-based model could be developed.

Intact porous rock in two or three dimensions cannot be modeled unless modifications are made to the compact base material to make it more porous. The summary of the microstructural physics of intact rock provided in Section 2 is intended to aid in the development of a model for intact porous rock. Preliminary work with the 2D flat-jointed material suggests that an acceptable model for intact porous rock can be created by adding initial slits and gaps to a well-connected flat-jointed material. The compression test response of the well-connected material differs from that of a typical porous rock (taken here to be Castlegate sandstone) in the following ways: (a) the axial stress versus axial strain curve is linear from the start of the test, whereas the Castlegate sandstone curve exhibits an initial hardening; (b) the Young's modulus does not increase with confinement; (c) the Poisson's ratio is too low; and (d) volumetric-strain reversal occurs at peak load, whereas it occurs well before peak load for Castlegate sandstone. It is expected that all of these discrepancies could be removed by modifying the initial microstructure to contain a mixture of bonded, slit, and gapped contacts. The slit contacts are unbonded and have an initial gap of zero, and the gapped contacts have a distribution of initial gap sizes. This capability is provided in Potyondy ([2014](#)). Ongoing development of a model for intact porous rock has been guided by matching the response during a thick-walled cylinder (TWC) test, in which a cylindrical specimen with an axially aligned hole is subjected to a pressure applied to the outside of the cylinder (Potyondy &

Xiao, [2014](#)). The response includes the TWC loading curve (pressure versus external volumetric strain) and damage formation at the inner-hole boundary.

All BPM modeling will benefit from the increase in computational speed that is provided by the multi-threading capability of PFC2D and PFC3D version 5.0. These PFC codes take advantage of multiple cores in an automatic fashion such that any existing model that runs on a single core will, without modification, run faster on multiple cores. With such continuing increases in computer power, bonded-particle modeling promises to become an increasingly important modeling approach to simulate boundary-value problems at a scale that appears in engineering and mining work.

Bonded-particle modeling is in an early phase of development. We have a generic model for intact compact rock and may soon have a generic model for intact porous rock. Future BPMs should be constructed to match particular rock types such as granite, limestone, or sandstone. The challenge is to keep the models as simple as possible by including only the features necessary to allow the relevant micromechanisms to occur. Haimson ([2007](#)) provides examples of all three of these rock types that demonstrate how subtle microstructural differences affect the macroscopic breakout behavior (e.g., the differing grain damage ahead of tabular slot-shaped breakouts in higher- and lower-porosity sandstones, as explained in Section 1). It should be possible to develop relatively simple BPMs that can capture these micromechanisms and thereby reproduce all of the macroscopic breakout behaviors.

References

Asadi, M. S., Rasouli, V., & Barla, G. (2012). A bonded particle model simulation of shear strength and asperity degradation for rough rock fractures. *Rock Mechanics and Rock Engineering*. doi:10.1007/s00603-012-0231-4

Bahrani, N., Potyondy, D., & Pierce, M. (2012). Simulation of brazilian test using PFC2D grain-based model. In *RockEng12 – rock engineering for natural resources. Proceedings of 21st Canadian rock mechanics symposium*, Edmonton, Canada, May 2012, pp. 485–493. Westmount: CARMA, CIMICM.

Bahrani, N., Valley, B., Kaiser, P. K., & Pierce, M. (2011). Evaluation of PFC2D grain-based model for simulation of

D.O. Potyondy

confinement-dependent rock strength degradation and failure processes. In *Proceedings of 45th U.S. rock mechanics/ geomechanics symposium*, San Francisco, CA, June 26–29, 2011, ARMA 11-156, CD.

Bandini, A., Berry, P., Bemporad, E., & Sebastiani, M. (2012). Effects of intra-crystalline microcracks on the mechanical behavior of a marble under indentation. *International Journal of Rock Mechanics and Mining Sciences*, *54*, 47–55.

Cho, N., Martin, C. D., & Sego, D. C. (2007). A clumped particle model for rock. *International Journal of Rock Mechanics and Mining Sciences*, *44*, 997–1010.

Cho, N., Martin, C. D., & Sego, D. C. (2008). Development of a shear zone in brittle rock subjected to direct shear. *International Journal of Rock Mechanics and Mining Sciences*, *45*, 1335–1346.

Cho, N., Martin, C. D., Sego, D. C., & Jeon, J. (2010). Dilation and spalling in axially compressed beams subjected to bending. *Rock Mechanics and Rock Engineering*, *43*, 123–133.

Costa, S., Kodikara, J., & Thusyanthan, N. I. (2008). Modelling of desiccation crack development in clay soils. In *Geomechanics in the emerging social and technological age. Proceedings 12th international IACMAG conference*, Goa, India, October 1–6, 2008, pp. 1099–1107, CD. Toronto: X-CD Technologies.

Cundall, P. A. (2011). Lattice method for modeling brittle, jointed rock. In D. Sainsbury, R. Hart, C. Detournay, & M. Nelson (Eds.), *Continuum and distinct element numerical modeling in geomechanics – 2011. Proceedings of 2nd international FLAC/DEM symposium*, Melbourne, Australia, February 14–16, 2011, pp. 11–19, ISBN 978-0-9767577-2-6. Minneapolis, MN: Itasca International.

Cundall, P. A., & Strack, O. D. L. (1979). A discrete numerical model for granular assemblies. *Géotechnique*, *29*, 47–65.

Damjanac, B., Board, M., Lin, M., Kicker, D., & Leem, J. (2007). Mechanical degradation of emplacement drifts at Yucca Mountain: A modeling case study, part 2: Lithophysal rock. *International Journal of Rock Mechanics and Mining Sciences*, *44*, 368–399.

Haimson, B. (2007). Micromechanisms of borehole instability leading to breakouts in rocks. *International Journal of Rock Mechanics and Mining Sciences*, *44*, 157–173.

Hazzard, J. F., Collins, D. S., Pettitt, W. S., & Young, R. P. (2002). Simulation of unstable fault slip in granite using a bonded-particle model. *Pure and Applied Geophysics*, *159*, 221–245.

Hazzard, J. F., & Young, R. P. (2000). Simulating acoustic emissions in bonded-particle models of rock. *International Journal of Rock Mechanics and Mining Sciences*, *37*, 867–872.

Hazzard, J. F., & Young, R. P. (2004). Dynamic modelling of induced seismicity. *International Journal of Rock Mechanics and Mining Sciences*, *41*, 1365–1376.

Holt, R. M., Kjolaas, J., Larsen, I., Li, L., Gotusso Pillitteri, A., & Sonstebo, E. F. (2005). Comparison between controlled laboratory experiments and discrete particle simulations of the mechanical behaviour of rock. *International Journal of Rock Mechanics and Mining Sciences*, *42*, 985–995.

Itasca Consulting Group, Inc. (2008). *PFC2D (particle flow code in 2 dimensions), version 4.0 [User's manual]*. Minneapolis, MN: ICG.

Itasca Consulting Group, Inc. (2011). *FLAC (fast lagrangian analysis of continua), version 7.0 [User's manual]*. Minneapolis, MN: ICG.

Itasca Consulting Group, Inc. (2014a). *PFC (particle flow code in 2 and 3 dimensions), version 5.0 [User's manual]*. Minneapolis, MN: ICG.

Itasca Consulting Group, Inc. (2014b). *UDEC (universal distinct element code), version 6.0 [User's manual]*. Minneapolis, MN: ICG.

Jaeger, J. C., Cook, N. G. W., & Zimmerman, R. W. (2007). *Fundamentals of rock mechanics* (4th ed.). Malden, MA: Blackwell.

Katsaga, T. (2010). *Geophysical imaging and numerical modelling of fractures in concrete* (doctoral dissertation). University of Toronto, Toronto.

Katsaga, T., & Potyondy, D. O. (2012). A generic stope model for investigation of fracturing mechanisms in deep gold mines. In *Proceedings of 46th U.S. rock mechanics/geomechanics symposium*, Chicago, USA, June 24–27, 2012, ARMA 12-541, CD.

Krajcinovic, D. (2000). Introduction to damage mechanics. In D. Krajcinovic & J. van Mier (Eds.), *Damage and fracture in disordered materials*. International Centre for Mechanical Sciences, CISM (pp. 1–15). Wien: Springer.

Kranz, R. L. (1983). Microcracks in rocks: A review. *Tectonophysics*, *100*, 449–480.

Lan, H., Martin, C. D., & Hu, B. (2010). Effect of heterogeneity of brittle rock on micromechanical extensile behavior during compression loading. *Journal of Geophysical Research*, *115*, B01202.

Lemos, J. V. (2011). Recent developments and future trends in distinct element methods: UDEC/3DEC and PFC codes. In *Proceedings 10th international conference on discontinuous deformation analysis*, ICADD-10, Hawaii, 2011.

Martin, C. D., & Chandler, N. A. (1994). The progressive fracture of Lac du Bonnet granite. *International Journal of Rock Mechanics and Mining Sciences*, *31*, 643–659.

Mas Ivars, D., Pierce, M. E., Darcel, C., Reyes-Montes, J., Potyondy, D. O., Young, R. P., & Cundall, P. A. (2011). The synthetic rock mass approach for jointed rock mass modelling. *International Journal of Rock Mechanics and Mining Sciences*, *48*, 219–244.

Mas Ivars, D., Potyondy, D. O., Pierce, M., & Cundall, P. A. (2008). The smooth-joint contact model. In B. A. Schrefler & U. Perego (Eds.), *Proceedings of WCCM8-ECCOMAS 2008: 8th world congress on computational mechanics/5th European congress on computational methods in applied sciences and engineering*, Venice, June 30–July 5, 2008 (Paper No. a2735). Barcelona: International Center for Numerical Methods in Engineering (CIMNE).

Meredith, P. G. (1990). Fracture and failure in brittle polycrystals: An overview. In D. J. Barber & P. G. Meredith (Eds.), *Deformation processes in minerals, ceramics and rocks*. London: Unwin Hyman.

Oreskes, N., Shrader-Frechette, K., & Belitz, K. (1994). Verification, validation, and confirmation of numerical models in the earth sciences. *Science*, *263*, 641–646.

Ostanin, I., Ballarini, R., Potyondy, D., & Dumitrica, T. (2013). A distinct element method for large scale simulations of carbon nanotube assemblies. *Journal of the Mechanics and Physics of Solids*, *61*, 762–782.

Park, J. -W., & Song, J. -J. (2009). Numerical simulation of a direct shear test on a rock joint using a bonded-particle model. *International Journal of Rock Mechanics and Mining Sciences*, *46*, 1315–1328.

Paterson, M. S., & Wong, T. -f. (2005). *Experimental rock deformation: The brittle field* (2nd ed.). Berlin: Springer.

Pierce, M. E., & Fairhurst, C. (2012). Synthetic rock mass applications in mass mining. In Q. Qian & Y. Zhou (Eds.), *Harmonising rock engineering and the environment*. Proceedings 12th ISRM international congress, Beijing, October 2011, pp. 109–114, ISBN 978-0-415-80444-8. London: Taylor & Francis Group.

Potyondy, D. (2009). *Simulating spalling, phase II: Feasibility assessment*. Itasca Consulting Group, Inc., Report to Svensk Kärnbränslehantering AB (SKB, Swedish Nuclear Fuel and Waste Management Company), Stockholm, Sweden, ICG09-2502-3F, January 2009.

Potyondy, D. (2014). *Material-modeling support in PFC*. Technical memorandum ICG7766-L, October 20, 2014. Minneapolis, MN: Itasca Consulting Group.

Potyondy, D., Cundall, P., DeGagne, D., & Corkum, A. (2008). *Simulating spalling, phase I: Pre-study*. Itasca Consulting Group, Inc., Report to Svensk Kärnbränslehantering AB (SKB, Swedish Nuclear Fuel and Waste Management Company), Stockholm, Sweden, ICG08-2468-1F, March 2008.

Potyondy, D., Ekneligoda, T., & Fälth, B. (2009). *Simulating spalling, phase II: Preliminary feasibility assessment*. Itasca Consulting Group, Inc., Report to Svensk Kärnbränslehantering AB (SKB, Swedish Nuclear Fuel and Waste Management Company), Stockholm, Sweden, ICG08-2502-5F, January 2009.

Potyondy, D., & Emam, S. (2008). *A particle-based model for studying excavation damage at Tournemire underground laboratory – phase I: Relevant mechanisms* (Itasca Consulting Group, Inc., Report to Institute of Radio-protection and Nuclear Safety (IRSN)), Fontenay-Aux-Roses Cedex, France, ICG08-2454-31, October 21, 2008.

Potyondy, D., & Emam, S. (2009). *A particle-based model for studying excavation damage at Tournemire underground laboratory – phase II: Hydric damage and tunnel simulations* (Itasca Consulting Group, Inc., Report to Institute of Radioprotection and Nuclear Safety (IRSN)), Fontenay-Aux-Roses Cedex, France, ICG09-2454-13, May 2009.

Potyondy, D. O. (2007a). Simulating stress corrosion with a bonded-particle model for rock. *International Journal of Rock Mechanics and Mining Sciences*, *44*, 677–691.

Potyondy, D. O. (2007b). The effect of voids on the mechanical properties of rock. In Cleary (Ed.), *Proceedings of 4th international conference on discrete element methods*, Brisbane, Australia. MEI Conferences, CD.

Potyondy, D. O. (2010a). *Molecular dynamics with PFC* (Technical Memorandum ICG6522-L, January 6, 2010). Minneapolis, MN: Itasca Consulting Group.

Potyondy, D. O. (2010b). *PFC2D grain-based models* (Technical Memorandum ICG6773-L, May 28, 2010). Minneapolis, MN: Itasca Consulting Group.

Potyondy, D. O. (2010c). *PFC2D grain-structure generator* (Technical Memorandum ICG6772-L, May 28, 2010). Minneapolis, MN: Itasca Consulting Group.

Potyondy, D. O. (2010d). A grain-based model for rock: Approaching the true microstructure. In C. C. Li, et al. (Eds.), *Rock mechanics in the Nordic countries 2010*. Proceedings of Bergmekanikk i Norden 2010, Kongsberg, Norway, June 9–12, 2010, pp. 225–234, ISBN: 978-82-8208-017-0. Kongsberg: Norwegian Group for Rock Mechanics.

Potyondy, D. O. (2011). Parallel-bond refinements to match macroproperties of hard rock. In D. Sainsbury, R. Hart, C. Detournay, & M. Nelson (Eds.), *Continuum and distinct element numerical modeling in geomechanics – 2011.*

Proceedings of 2nd international FLAC/DEM symposium, Melbourne, Australia, February 14–16, 2011, pp. 459–465, ISBN 978-0-9767577-2-6. Minneapolis, MN: Itasca International.

Potyondy, D. O. (2012). A flat-jointed bonded-particle material for hard rock. In *Proceedings of 46th U.S. rock mechanics/geomechanics symposium*, Chicago, USA, June 24–27, 2012.ARMA 12-501, CD.

Potyondy, D. O., & Cundall, P. A. (2004). A bonded-particle model for rock. *International Journal of Rock Mechanics and Mining Sciences*, *41*, 1329–1364.

Potyondy, D. O., & Hazzard, J. F. (2008). Effects of stress and induced cracking on the static and dynamic moduli of rock. In R. Hart, C. Detournay, & P. Cundall (Eds.), *Continuum and distinct element numerical modeling in geo-engineering 2008. Proceedings of 1st international FLAC/DEM symposium*, Minneapolis, MN, USA, August 25–27, 2008, pp. 147–156. Minneapolis, MN: Itasca Consulting Group.

Potyondy, D. O., & Xiao, Y. (2014). Simulating perforation damage with a flat-jointed bonded-particle material. *International Journal of Rock Mechanics and Mining Sciences*. Pending approval by BP, manuscript dated September 4, 2014.

Rapaport, D. C. (2004). *The art of molecular dynamics simulation* (2nd ed.). Cambridge: Cambridge University Press.

Rejeb, A., & Cabrera, J. (2006). Time-dependent evolution of the excavation damaged zone in the argillaceous tournemire site (France). In W. Xu, X. Tan, & S. Yang (Eds.), *Advances on coupled thermo-hydro-mechanical-chemical processes in geosystems and engineering. Proceedings of GEOPROC 2006*, Nanjing, China, May 2006, pp. 65–74. Nanjing: HoHai University.

Schöpfer, M. P. J., Abe, S., Childs, C., & Walsh, J. J. (2009). The impact of porosity and crack density on the elasticity, strength and friction of cohesive granular materials: Insights from DEM modelling. *International Journal of Rock Mechanics and Mining Sciences*, *46*, 250–261.

Schöpfer, M. P. J., Arslan, A., Walsh, J. J., & Childs, C. (2011). Reconciliation of contrasting theories for fracture spacing in layered rocks. *Journal of Structural Geology*, *33*, 551–565.

Schöpfer, M. P. J., & Childs, C. (2013). The orientation and dilatancy of shear bands in a bonded particle model for rock. *International Journal of Rock Mechanics and Mining Sciences*, *57*, 75–88.

Schöpfer, M. P. J., Childs, C., & Manzocchi, T. (2013). Three-dimensional failure envelopes and the brittle–ductile transition. *Journal of Geophysical Research*, *118*, 1378–1392.

Schöpfer, M. P. J., Childs, C., & Walsh, J. J. (2007a). 2D distinct element modeling of the structure and growth of normal faults in multilayer sequences, part 1: Model calibration, boundary conditions and selected results. *Journal of Geophysical Research*, *112*, B10401.

Schöpfer, M. P. J., Childs, C., & Walsh, J. J. (2007b). 2D distinct element modeling of the structure and growth of normal faults in multilayer sequences, part 2: Impact of confining pressure and strength contrast on fault zone geometry and growth. *Journal of Geophysical Research*, *112*, B10404.

Stafford, W. (1998). What's in my journal. In P. Merchant & V. Wixon (Eds.), *Crossing unmarked snow: Further views on the writer's vocation*. Ann Arbor: University of Michigan Press.

Starfield, A. M., & Cundall, P. A. (1988). Towards a methodology for rock mechanics modelling. *International Journal of Rock Mechanics and Mining Sciences*, *25*, 99–106.

van Mier, J. G. M. (2007). Multi-scale interaction potentials (F-r) for describing fracture of brittle disordered materials like cement and concrete. *International Journal of Fracture, 143*, 41–78.

Wanne, T. S., & Young, R. P. (2008). Bonded-particle modeling of thermally fractured granite. *International Journal of Rock Mechanics and Mining Sciences, 45*, 789–799.

Wikipedia. (2012). Entry for "Ab initio" on 17 August 2012.

Winsberg, E. (2010). *Science in the age of computer simulation*. Chicago, IL: University of Chicago Press.

Yoon, J. S., Zang, A., & Stephansson, O. (2012). Simulating fracture and friction of Aue granite under confined asymmetric compressive test using clumped particle model. *International Journal of Rock Mechanics and Mining Sciences, 49*, 68–83.

Zhang, F., Huang, H., & Damjanac, B. (2012). DEM/pore network modeling of fluid injection into granular media. In *Proceedings 46th U.S. Rock mechanics/geomechanics symposium*, Chicago, USA, June 24–27, 2012, ARMA 12-621, CD.

Zöllner, D. (2006). Construction of polycrystalline microstructures. In *Workshop in Bad Helmstedt*, November 24, 2006. Retrieved April 26, 2010 from http://www.uni-magdeburg.de/gkmm/Folien/zoellner.ppt